Supramolecular Presentation of Hyaluronan onto Model Surfaces for Studying the

Behaviour of Cancer Stem Cells

Xinqing Pang, Clare O'Malley, João Borges, Muhammad M. Rahman, Dominic W. P. Collis,

João F. Mano, Ian C. Mackenzie, Helena S. Azevedo*

Xinqing Pang, Dr. C. O'Malley, Dr. D. W. P. Collis, Dr. H. S. Azevedo

School of Engineering and Materials Science, Institute of Bioengineering, Queen Mary

University of London, E1 4NS, UK

Email: h.azevedo@qmul.ac.uk

Dr. J. Borges, Prof. J. F. Mano

Department of Chemistry, CICECO – Aveiro Institute of Materials, University of Aveiro, 3810-

193 Aveiro, Portugal

Dr. M. M. Rahman, Prof. I. C. Mackenzie

Blizard Institute, Barts and The London School of Medicine and Dentistry, Queen Mary

University of London, E1 2AT, UK

The supramolecular presentation of extracellular matrix components on surfaces provides a

platform for the investigation and control of cell behaviour. Hyaluronan (HA) is one of the

main components of the extracellular environment and has been shown to play an

important role in different cancers and their progression. However, current methods of HA

immobilisation often require its chemical modification. Herein, a peptide-based self-

assembled monolayer (SAM) is used as an anchor to immobilise unmodified HA on a bare

gold surface, as demonstrated by the quartz crystal microbalance with dissipation

monitoring. Peptide-HA surfaces show increased roughness and greater hydrophobicity when compared to poly-D-lysine/HA surfaces, as measured by atomic force microscopy (AFM) and water contact angle, respectively. Additionally, the peptide SAM can be micro-contact printed and used to restrict the presentation of HA to specific regions, thereby creating HA patterned surfaces to examine cell behaviour. When used for cell culture, these surfaces result in altered adhesion and migration of LUC4 head and neck squamous cell carcinoma cells. These biomimetic surfaces can provide insights into the role of HA in cancer and other diseases and be used as platform for the development of cell sorting devices.

1. Introduction

The ability to fabricate well-defined surfaces to control and investigate cell behaviour provides a useful tool for *in vitro* cell culture. For instance, it is increasingly important for the regulated production of *in vitro*-expanded or differentiated cells for cell-based therapies. In this regard, self-assembled monolayers (SAMs) can provide a rapid and simple method for fabricating well-ordered surfaces with a wide range of functionalities.

SAMs provide a useful platform for high-throughput screening of peptide-cell interactions to identify surfaces able to elicit the desired effect on cells in culture.[1] They have been successfully employed to influence cell adhesion, support proliferation, and direct differentiation or even maintain the pluripotency of stem cells.[2] One potential benefit of using SAMs in cell expansion is the elimination of the need for animal-derived products to support the cell proliferation crucial for the expansion of cells to be used in cellular therapies.

The interaction between SAMs and cell culture components, in the form of either cells or serum proteins, can be exploited to examine in more detail the role of such proteins in guiding cell fate. For example, how the conformation of adsorbed fibronectin impacts the way in which it interacts with cells.[2d, 3] In addition, the density and spacing of functional groups can be precisely controlled[4] and the use of micro-contact printing (μCP) enables SAMs to be formed in discrete patterns, which can be used to further regulate cell adhesion and even migration.[5]

However, the use of SAMs for the non-covalent immobilisation of individual extracellular matrix (ECM) components is less frequently used. Hyaluronic acid (HA) is the only non-

sulfated glycosaminoglycan (GAG) which comprises a large part of the ECM of many tissues. It is made up of alternating D-glucuronic acid and *N*-acetyl-D-glucosamine monomers, containing both hydrophilic and hydrophobic patch domains.[6] While the hydrophilic carboxyl, hydroxyl and acetamido groups confer high water solubility to HA, the hydrophobic regions, created by axial hydrogen atoms, can reversibly interact with each other to form a meshwork. In addition, hydrogen bonding between the hydrophilic side groups contributes to the porous mesh-like structure, which is formed in solution and retains water. Internal swelling pressure is generated on compression of HA networks and, when this pressure is released, mutual repulsion between carboxyl groups allows a return to its original shape.[7] *In vivo*, this is a key characteristic which significantly contributes to the viscoelastic properties of several tissues, including cartilage[8] and the vitreous humour.[9]

In addition to its biophysical characteristics, HA itself interacts with cells via cell-surface receptors such as CD44 and receptor for hyaluronan-mediated motility (RHAMM).[7] HA is also known to accumulate in the tumour microenvironment and, signalling via these receptors, can support metastasis, cancer cell proliferation, and multidrug resistance.[10] Within head and neck squamous cell carcinoma (HNSCC) there is a sub-population of stem-like cells (herein referred to as cancer stem cells or CSCs) with tumour-initiating potential and the ability to restore tumour heterogeneity.[11] These cells are thought to play an important role in tumour progression and are identified predominantly by their higher CD44 expression levels.[11-12] It has been demonstrated that signalling downstream of HA-CD44 interactions can regulate stem cell markers and highlights the role of HA in HNSCC progression.[13]

Due to the pivotal role of HA in many cellular processes, numerous methods have been developed to immobilise HA on surfaces, aiming to study its effects in a 2D *in vitro* cell culture environment. These approaches often require the chemical modification of native HA by biotinylation,[14] conjugation to dopamine,[15] thiolation,[16] azidation,[17] or functionalisation of surfaces to allow the covalent attachment of HA.[18]

However, such modifications can interfere with the native properties of HA. For example, thiolation has been shown to inhibit HA degradation by hyaluronidases,[19] and influence its conformation once immobilised. Altered presentation of macromolecules has been shown to affect cell adhesion and highlights the sensitivity of mammalian cells to their culture environment and the importance of creating well-defined surfaces for *in vitro* studies of cell behaviour.[3, 20]

Herein, we propose a straightforward platform for the immobilisation of HA in its native form on a gold (Au) surface using a SAM consisting of a thiolated HA-binding peptide.[21] To the best of our knowledge, the supramolecular assembly of HA using HA-binding peptides has not yet been exploited to study the effects of immobilized HA on cancer stem cells. We believe that this approach provides important advantages over the aforementioned methodologies. Firstly, it does not require any covalent modification of HA, thus allowing a more biomimetic presentation, reminiscent of the natural ECM. Secondly, our method is simple and rapid, while offering precise control over HA presentation, which is highly advantageous when attempting to control cell fate.

2. Results and Discussion

2.1. Thiolated HA-binding peptide for the supramolecular presentation of HA

In this work, we have taken a 12-amino acid HA-binding peptide identified through phage display, named Pep-1, to produce SAMs on Au surfaces via peptide thiolation at the N-terminal **(Figure S1-S3)**. This peptide has a distinct sequence which does not contain the consensus domain observed in several HA-binding proteins, including CD44 and RHAMM.[21] The assessment of the peptide's binding ability to HA-coated beads has revealed a dissociation constant (K_d) value of ~ 1.65 µM.[21] Studies into the function and effects of Pep-1 have been conducted,[22] demonstrating its ability to bind HA in solution, immobilised on a surface, or in complex with cells both *in vitro* and in tissue sections.[23] On binding, Pep-1 influences HA-mediated signalling and has been used as an inhibitor of HA function.[24] It has previously been modified and subsequently used to form a peptide layer on human cartilage samples and contact lenses, which sequestered HA and resulted in an enhanced surface lubrication and water retention.[25] The covalent bond between thiol groups and Au is well-known and often used in the formation of SAMs on Au substrates. As such, we expect that the thiolated Pep-1 (herein referred to as HS-Pep-1) will form a monolayer on Au, which can be used to further immobilise HA in its native form. **Scheme 1** illustrates the proposed model for HS-Pep-1 SAM formation (Scheme 1B) on an Au surface (Scheme 1A) and the subsequent immobilisation of HA (Scheme 1C) and interaction with mammalian cells (Scheme 1D). To confirm that the HS-Pep-1 successfully binds to the Au substrate, we used both the quartz crystal microbalance with dissipation monitoring (QCM-D) and the water contact angle to quantify changes in the film's hydrated thickness and areal mass density, as well as in the surface hydrophobicity, respectively.

Using QCM-D apparatus, a decrease in the resonance frequency normalised to the 7th overtone ($n = 7$; 35 MHz; $\Delta f_7/7$) was observed as a function of time, following the addition of

a 0.01 mM aqueous solution of HS-Pep-1 (-18.7±1.2 Hz). This decrease in the $\Delta f_7/7$ was maintained following the washing step **(Figure 1A)**, which reveals the strong adsorption of the HS-Pep-1 layer onto the Au surface. At the same time, a negligible shift in the energy dissipation factor was obtained at the 7th overtone ($\Delta D_7 < 0.3 \times 10^{-6}$). The very low dispersion in the $\Delta f_n/n$ confirms that HS-Pep-1 adsorbs rigidly onto the Au surface **(Figure S4)**.

Therefore, the adsorbed HS-Pep-1 layer can be considered as a rigid film and, thus, the Sauerbrey equation can be used to estimate the areal mass density of the adsorbed HS-Pep-1 layer ($\Delta m_{Sauerbrey} = 329.6 \pm 65.5$ ng/cm^2). Based on this assumption, the QCM-D data and the Sauerbrey relationship were also used to estimate the thickness of the adsorbed HS-Pep-1 layer ($h_{Sauerbrey} = 3.3 \pm 0.6$ nm). However, as the film is hydrated, one should bear in mind that the obtained areal mass density of the film may include the mass of the adsorbed layer plus coupled solvent. Therefore, for comparison, the areal mass density and hydrodynamic thickness of the adsorbed HS-Pep-1 layer were also estimated using the Voigt-based viscoelastic model **(Table 1)**, reaching values of 354.1±96.6 ng/cm^2 (Δm_{Voigt}) and 3.7±1.0 nm (h_{Voigt}), respectively. These values are in the range of those obtained using the Sauerbrey model, thus meaning that the obtained areal mass density and thickness are mainly assigned to the adsorption of the HS-Pep-1 layer, and the effect of the coupled solvent can be considered negligible.

A decrease in the $\Delta f_7/7$, and thus increase in the areal mass density, as well as an increase in the ΔD_7 was seen after the adsorption of the HA biopolymer (1.5 MDa) onto the HS-Pep-1-coated Au surface, reaching values of -9.1±2.7 Hz and (1.8±0.2) ×10^{-6}, respectively (Figure 1A). The overtones become separated after the addition of the HA layer, which is a typical behaviour of a soft and hydrated film (**Figure S5**). This reveals the viscoelastic behaviour of

the adsorbed HA layer, which is a common characteristic of most polymeric systems.[26]

Therefore, the Voigt-based viscoelastic model was used to estimate the areal mass change

(1154.0 ± 492.1 ng/cm^2) and the hydrodynamic thickness (10.8 ± 4.8 nm) of the adsorbed 1.5

MDa HA layer (Table 1). For comparison, when the acetylated Pep-1 (herein referred to as

Ac-Pep-1) was used, i.e. without the thiol group, a smaller decrease in the $\Delta f_7/7$ (-10.5 Hz)

was seen, which was maintained upon washing (Figure 1B). To explain these results, we

hypothesise that the Ac-Pep-1 was able to interact with the bare Au surface through the

positively charged arginine residues (i.e. amino groups) at the *C*-terminal of the peptide.

This would also explain the lack of adsorption of the negatively charged HA onto the Ac-Pep-

1-modified Au surface as the amino groups would be inaccessible and the acetyl groups will

not interact with the HA (Figure 1B).

In addition to the observed changes in the normalised frequency and energy dissipation

shifts, the water contact angle decreased from 76.9 ± 6.2 ° on bare Au, to 66.7 ± 2.7 ° after

incubation with a 1 mM ethanolic solution of HS-Pep-1 (Figure 1D, E). This indicates an

increase in the hydrophilicity and a change in the surface chemistry of the Au, through HS-

Pep-1 deposition.

A further reduction in the water contact angle to 57.9 ± 4.2 ° was observed when the

surfaces coated with the HS-Pep-1 SAM were exposed to an aqueous solution of 1.5 MDa

HA (Figure 1D, E), indicating that the overall surface became more hydrophilic. This

decrease in hydrophobicity upon HA binding was expected due to the high number of

hydroxyl and carboxyl groups present in HA which confer its high water solubility. This value

is higher than those reported in the literature, where values of 24.8 ± 0.1 ° and 12.8 ± 0.6 °

were obtained for similar HA-coated surfaces. However, in those cases HA was immobilised

by co-deposition with poly-dopamine or by covalent attachment to the Au surface, respectively.[15b, 18a] Such differences in the immobilisation methodologies could be proposed as the main reason for the discrepancy between these values and the ones obtained in the current study.

The direct exposure of the Au surface to an aqueous solution of HA, in the absence of a HS-Pep-1 SAM, did not result in a change in the water contact angle (Figure 1D, E) or deposition onto the bare Au surface **(Figure S6)**.

Taken together, these results demonstrate that the immobilisation of HS-Pep-1 onto the Au surface leads to a rigid film and does not inhibit its ability to bind HA through the arginine residues at the *C*-terminal. Hence, it can be used for the supramolecular presentation of HA on the Au surface. This system would be advantageous over other platforms for *in vitro* cell culture studies due to the ease of HS-Pep-1 monolayer formation without loss of HA-binding ability. Moreover, it does not require multi-step chemical modification of the surface or the covalent modification of HA. The supramolecular immobilisation involves weaker attractive forces, such as electrostatic interactions between negatively charged HA and the positively charged HS-Pep-1-modified Au surface, thereby producing a more physiologically relevant supramolecular platform, reminiscent of the native ECM, for the investigation of cell behaviours.

2.2. HA immobilisation using HS-Pep-1 and poly-D-lysine model surfaces

To probe any differences in HA deposition between our system and existing methods, poly-lysine was used as a model surface for comparison. Poly-lysine is a positively charged hydrophilic polyelectrolyte at a physiological pH (pKa ~10.5[27]) and is frequently used in layer-by-layer assembly studies in combination with oppositely charged polymers, including

HA.[28] Poly-lysine readily adsorbs onto the prepared surfaces and, due to its positive charge, can immobilise HA through attractive electrostatic interactions. As reported in the literature, poly-D-lysine (PDL) has been used to minimise any degradation of adsorbed layers by inherent cellular enzyme activity.[29]

The QCM-D data showed a decrease in the $\Delta f_7/7$ signal and an increase in ΔD_7 when the aqueous solution of PDL was introduced into the system, which demonstrates the adsorption of PDL onto the bare Au surface (Figure 1C). Again, the rinsing step led to negligible changes in both the $\Delta f_7/7$ and ΔD_7 values, thus suggesting the strong association of the PDL, as well as the irreversible nature of the adsorption process. A further decrease in the $\Delta f_7/7$ was observed after the addition of an aqueous solution of 1.5 MDa HA onto the PDL-modified Au surface, indicating HA immobilisation (Figure 1C). The comparison of the deposition of HA onto the HS-Pep-1 (Figure 1A) and PDL (Figure 1C) modified Au surfaces reveals a greater decrease in the $\Delta f_7/7$ signal for the adsorption of HA onto the PDL-modified Au surface, -9.1±2.7 Hz compared with -16.1±0.3 Hz, respectively. The Voigt-based viscoelastic model was used to determine the areal mass density and hydrodynamic thickness of the HA layer adsorbed onto PDL, reaching values of 1342.0±653.7 ng/cm^2 and 12.1±6.6 nm, respectively (Table 1).

The average water contact angle of the PDL-coated Au was 25.4±8.6°, which did not change significantly on incubation with HA, 21.8±5.8°, indicating a highly hydrophilic surface (Figure 1D, E). These results demonstrate that the immobilisation of HA by HS-Pep-1 SAM creates a surface with lower hydrophilicity when compared with its immobilisation by PDL. The sequence of HS-Pep-1 (Figure S1A) contains several hydrophobic domains, indicating that it is less hydrophilic when compared to PDL. The higher contact angle observed for the HS-

Pep-1-HA surface, when compared to PDL-HA surface, might be due to the conformation of HA upon binding to the Pep-1 SAMs, whereby HA hydrophobic regions are more exposed at the surface.

2.3.   Effect of HA molecular weight on immobilisation

HA of different molecular weight (MW) has been shown to elicit different effects on cell behaviours both *in vitro* and *in vivo*, where lower but not high MW can induce maturation of dendritic cells, stimulate angiogenesis, and are known to be immunogenic.[30] Using QCM-D, we have further analysed the effect of the MW of HA (20 kDa, 200 kDa and 1.5 MDa) on its immobilisation by the HS-Pep-1 SAM or PDL (Figure S5). The average final mass deposition of HA, following the washing step was not statistically different between the three sizes of HA used when immobilised by the HS-Pep-1 SAM. However, significantly more 1.5 MDa HA was immobilised onto PDL than 20 and 200 kDa HA **(Figure 2A)**. The HA layer formed on the HS-Pep-1 SAM or PDL was assessed using the Voigt-based viscoelastic model. No significant difference was observed between the three different MWs adsorbed onto HS-Pep-1 modified Au surfaces, with the thicknesses ranging from 5.4±1.8 (20 kDa HA) to 10.8±4.8 (1.5 MDa HA) nm. However, the thickness of the 1.5 MDa HA layer on PDL was 12.1±6.6 nm, which was significantly thicker than the layers formed by the 20 and 200 kDa HA (Table 1).

In addition, there was a trend towards a greater mass and, to a lesser extent, thickness (Figure 2A and B respectively) with increasing MW of HA. This could be explained by HA adsorbing onto the substrates through a similar number of contact points. However, the increase in chain length of the higher MW HA would mean a larger amount of HA more loosely attached to the surface, extending out into the surrounding solution, resulting in both an increased mass and thicker layer.

Along with the information on the areal mass density, the QCM-D also provides information on the viscoelastic properties of HS-Pep-1-HA and PDL-HA films.[31] Figure 2C shows the mean change in the dissipation factor following the incubation of HS-Pep-1- and PDL-modified Au surfaces with HA of different MW. The increase in dissipation factor values indicates that the HA-based films are softer than the HS-Pep-1 or PDL layers alone.[32] No statistically significant differences between the ΔD values observed for PDL immobilisation of HA compared to HS-Pep-1 were seen (Figure 2C). However, the MW of HA was shown to influence the viscoelastic properties, resulting in a softer film when a higher MW was used. This is likely due to the hydration of the film, where larger HA molecules will be able to incorporate more water into the adsorbed layer.

2.4. Topography and patterning of HA surfaces

Atomic force microscopy (AFM) was used to assess the topographical features of the films in dried and hydrated states (**Figure 3A-D**). It was seen that the average roughness of the single HS-Pep-1 or PDL layer in air was 4.85±2.16 and 3.77±1.78 nm, respectively **(Figure S7)**. On incubation with 1.5 MDa HA, the average roughness in air was measured as 4.59±3.12 nm for the HS-Pep-1-HA surface and 2.96±1.00 nm for the PDL-HA **(Figure 3A-B, E)**, being consistent with previous values reported for PLL-HA (1.5 MDa) system.[33] In both cases, the average roughness decreased after the deposition of HA **(Figure S7D)**.

Since the intended application of the developed surfaces is cell culture studies, and these are performed in an aqueous environment, the roughness of HS-Pep-1-HA and PDL-HA surfaces was also assessed in a hydrated state. No significant change in roughness was seen between the dry and hydrated surface when HA was immobilised by PDL **(Figure 3E)**. A significant increase in average roughness was observed when the HS-Pep-1-HA sample was

hydrated, from 4.59±3.12 nm to 31.08±36.12 nm. We hypothesise that, when dried, the polymers making up the coating will sit close to the Au surface, whereas, when hydrated long HA chains could extend out into the solution from the surface resulting in increased roughness, as supported by studies in the literature.[34]

The hydrated HS-Pep-1-HA samples were also significantly rougher than the hydrated PDL-HA surface (Figure 3C-E). The difference in roughness suggests that the mechanism and strength of binding is influencing the presentation of HA.

The strong attractive electrostatic interaction between the positively charged PDL and the negatively charged HA chains is assumed to be distributed evenly along both molecules, creating a coating which can uniformly resist the increased forces following swelling resulting in a smoother surface. Whereas HS-Pep-1 binding to HA occurs at discrete sites on the HA polymer, resulting in more free ends or segments of HA which could account for the increased surface roughness observed.

Patterned surfaces are a useful tool in cell culture and can be used to influence cell survival, adhesion, proliferation, migration, and differentiation.[35] As such, PDMS stamps were used to μCP the HS-Pep-1 onto the bare Au substrate. Incubation with Texas Red labelled HA resulted in deposition in distinct foci **(Figure 4C)** or as a background of HA with patches of bare Au creating a pattern (Figure 4D). This demonstrates a simple and rapid method for creating HA patterned surfaces with thiolated HA-binding peptide (HS-Pep-1, Figure 4A).

2.5. Interaction of immobilized HA with hyaladherins and serum proteins

The presence of HA on Pep-1 SAMs was shown via micro-contact printing of HS-Pep1 patterns and localization of fluorescently-labelled HA on printed patterns (Figure 4C, D). To

further demonstrate the ability of immobilized HA to be recognized by hyaladherins (HA-binding proteins, HABPs), binding studies using biotinylated HABPs (biotinylated G1 domain of aggrecan and biotinylated link protein) were performed. Incubation of surfaces with HA immobilized on Pep-1 patterns with biotin-HABP, and subsequently with Texas Red tagged avidin, revealed the accumulation of red fluorescence on the patterned areas **(Figure S8E, F).** In contrast, no fluorescence was detected on the various control surfaces (HA on gold or immobilized onto PDL, Pep-1 SAMs only, and alginate immobilized on Pep-1 SAMs, Figure S8A-D). Since PDL does not bind strongly to Au, the PDL patterns are not stable enough to withstand the various washing steps used in the binding assay with HABP. As result, the weak fluorescence observed is not restricted within the patterned areas (Figure S8D). QCM-D experiments on the immobilization of alginate (a negatively charge polysaccharide) on Pep-1 SAMs showed mass deposition (Δm = 2807.5±192.5 ng/cm^2) that was slightly removed upon washing **(Figure S9)**. Incubation of surfaces with alginate immobilized on Pep-1 SAMs with HABP did not show fluorescence accumulation areas (Figure S8C), confirming the specificity of HABP for HA. Furthermore, incubation of HABP on patterned Pep-1 SAMs areas (Figure S8B), without HA, also did not reveal enhanced fluorescence. Taken together, these results proved the presence of HA bound to Pep-1 SAMs and its binding to hyaladherins. The next step was to gain insights on the interactions of HA surfaces with serum proteins, which is key to understand cell behaviour on the HA surfaces. Protein adsorption studies on HA layers immobilized on HS-Pep-1 and PDL surfaces were carried out by QCM-D. Single protein solutions, bovine serum albumin (BSA, 0.5 mg/mL), and mixture of proteins, foetal bovine serum (FBS, 10%) were selected for these studies. Albumin is the most abundant protein in the human blood plasma and accounts for 55% of the total protein content (35-50 mg/mL), being negatively charged at neutral pH. QCM-D

14

results indicate an areal mass density of $\Delta m = 185.0 \pm 46$ ng/cm^2 for BSA deposition over HA immobilized on Pep-1 SAMs **(Figure S10, Table S1)**. BSA adsorption on HA-free Pep-1 SAMs (**Figure S11**, Table S1) was also performed with $\Delta m = 710.0 \pm 171.9$ ng/cm^2 which is substantially higher than the value obtained for the HS-Pep-1-HA surfaces. This higher value might be due to strong attractive electrostatic interactions between the negatively charged BSA and the positive *C*-terminal end on the Pep-1 SAM. Studies on the adsorption of proteins on HA immobilized surfaces have shown distinct results. For example, QCM-D experiments on BSA (5 mg/mL) over end-thiolated HA immobilized on Au surfaces, and end-alkylated or side-alkylated HA tethered to alkanethiols carrying oligo(ethylene gycol) with azide termini, showed no deposition of BSA onto these surfaces.[16] In another study, BSA (1 mg/mL) adsorption onto surfaces spin-coated with photoreactive HA (modified with 4-azidoaniline) and UV-crosslinked, monitored by QCM-D, revealed significant levels of albumin adsorption (~250 ng/cm^2).[17] However, different immobilization methods and BSA concentrations were used, being difficult to compare results among the different studies. The adsorption of proteins from FBS used in cell culture on the various surfaces was also monitored by QCM-D (**Figures S12-S14**). Higher levels of mass deposition were observed for serum proteins when compared to BSA adsorption onto the same surfaces (Table S1). However, the calculated masses for the HA-coated surface was lower than for the surface containing only Pep-1 SAMs. These differences in protein adsorption on the various surfaces further confirm the presence of HA over the Pep-1 SAMs. The results also infer that HA hydrophobic regions might be exposed at surface while its negatively charged carboxylate groups are engaged with amine groups of the terminal arginine in Pep-1 SAMs.

2.6. *In vitro* culture of head and neck cancer cells on HS-Pep-1-HA surfaces

The use of HA immobilized on surfaces to study interactions with cancer cells has been reported in few studies. For instance, the effect of HA MW on gastric cancer cells was investigated by immobilizing HA through PLL and combining layer-by-layer assembly and crosslinking approaches.[33] HA-patterned surfaces were also fabricated to present HA in discrete regions and study the behaviour of colon and breast cancer cells on the HA patterns.[36] To demonstrate the utility of the HA functionalized surfaces developed in this work, they were further applied to study the behaviour of CSCs in oral squamous cell carcinoma (OSCC). CSCs in OSCC were shown to switch between two sub-populations, proliferative epithelial CSCs (CD44$^+$EpCAM^{high}) and migratory/metastasis post-EMT CSCs (CD44^{high}EpCAM^{low-}) by undergoing epithelial-to-mesenchymal transition (EMT) and mesenchymal-to-epithelia transition (MET).[37]

Immortalised CA1 and LUC4 OSCC cell lines were selected as both produce EMT cells. LUC4 cells produce significantly more EMT cells than CA1 as shown in the FACS plots (**Figure S15**, 0.39% CA1 and 30.11% in LUC4). Cells were first cultured on the various surfaces for different periods of time. After 4 days, CA1 cells formed colonies on bare glass and have EMT cells present **(Figure S16)**. However, in Pep-1 SAM and HA immobilized surfaces fewer colonies, which appeared less densely packed, and a greater number of single cells were observed. LUC4 cells, which produce more EMT cells, showed a similar behaviour. Cells were then stained with vimentin (VIM) and cytokeratin (CK) which are positive markers for EMT and epithelial cells, respectively. A large number of EMT cells were found in LUC4 cells cultured on Pep-1 SAM and HA immobilized surfaces **(Figure 5)**. Flow cytometry was performed to identify the epithelial and EMT fractions of CA1 and LUC4 cells as CD44^{high} cells that lose epithelial cell adhesion molecule (EpCAM) expression and assess the binding

16

of HA to these cells (Figure S15). HA-FA was found to bind to both epithelial and EMT cells in both cell lines, but the EMT fraction of LUC4 cells was still distinguishable by loss of EpCAM expression. Based on these results, time-lapse microscopy was performed on LUC4 cells seeded on glass slides with Au-coated stripes containing immobilized HA via Pep-1 SAMs. While there was no migration of cells from the glass (brighter area) towards the HA stripes (darker area, video in supporting information), cells on the HA areas remained attached, showed a more elongated morphology **(Figure 6)** and displayed constant shifting to and from an EMT phenotype. Cells on the bare glass remained rounded and were migrating, but rarely underwent EMT (video in supporting information).

3. Conclusion

In this work we demonstrate the supramolecular immobilisation of unmodified HA on Au surfaces using a thiolated HA-binding peptide. This method produces surfaces which are distinct when compared to the immobilisation of HA by PDL. In addition, it allows a simple, rapid, and efficient way of creating HA-patterned surfaces, which were used to further probe the effect of HA on cells *in vitro*. The results suggest the potential of HA-patterned surfaces for cell sorting applications.

4. Experimental Section

Preparation of 3-(((4-methoxyphenyl)diphenylmethyl)thio)propanoic acid:

3-mercaptopropanoic acid (Sigma-Aldrich, USA, 9.4 mmol) was added dropwise to a solution of Mmt-Chloride (Sigma-Aldrich, 11.33 mmol), *N*,*N*-Diisopropylethylamine (DIPEA, Alfa Aesar, USA, 16.0 mmol) and dichloromethane (DCM, Sigma-Aldrich)/dimethylformamide (DMF, VWR, USA) in a 1:1 ratio and stirred overnight. The reaction mixture was suspended in deionized H_2O and then washed 3 times in an equal volume of ether. The organic layer as

washed with brine, dried over MgSO$_4$ (Fisher Scientific, USA), reduced under negative pressure and dried under vacuum. The final product was analysed by nuclear magnetic resonance (NMR, **Figure S1**).

Peptide synthesis:

Pep-1 (GAHWQFNALTVR) was synthesised in the Liberty Blue automated microwave peptide synthesiser (CEM, UK) using the standard 9-fluorenyl methoxycarbonyl (Fmoc) solid phase chemistry.[38] Pep-1 was capped at the N-terminal, either with an acetyl group **(Figure S2A)**, by shaking twice for 20 minutes with acetic anhydride 10% in DMF (w/v), or with 2-fold excess of 3-(((4-methoxyphenyl) diphenylmethyl)thio)propanoic acid (Figure S2B) following the same coupling procedure as for the protected amino acids. Peptides were then cleaved using a solution of trifluoroacetic acid (TFA) (Sigma-Aldrich), triisopropylsilane (Alfa Aesar) and water (95:2:5:2.5) for acetylated peptides, or TFA, thioanisole (Sigma-Aldrich), anisole (Sigma-Aldrich) and EDT (Sigma-Aldrich) (90:5:2.5:2.5) for thiolated peptides. Crude peptides were purified using preparative reverse-phase high performance liquid chromatography (RP-HPLC, C18 XBridge column, Waters, UK) on a gradient of 98% H$_2$O to 100% acetonitrile (Sigma-Aldrich) supplemented with 0.1 % TFA over 30 minutes using a flow rate of 20 mL/min. Purified product was collected based on the peptide mass, as detected by the SQ Mass Detector (Waters), reduced under negative pressure and then lyophilised. Peptide mass and purity were confirmed by mass spectrometry (**Figure S3A, B**) and HPLC (Figure S3C, D) analysis, respectively.

Fluorescent labelling of HA:

Texas red was conjugated to HA (Figure 4B) as previously described.[10d] Briefly, 1.5 MDa HA (Lifecore Biomedical, USA) was dissolved in 20 mM MES (Sigma) pH 4.5, 30% ethanol

(Sigma-Aldrich), and 3 times excess *N*-(3-Dimethylaminopropyl)-*N'*-ethylcarbodiimide hydrochloride (EDCI, Sigma-Aldrich) related to the number of HA disaccharide units. Texas Red hydrazide (Molecular Probes, Invitrogen, UK) was dissolved in DMF and added to the HA mixture at a molar ratio of fluorophore to disaccharide number of 1:10 and incubated at room temperature with shaking, overnight in the dark. The solution was dialysed against 75 mM NaCl (Fisher Scientific), in 40% ethanol, using regenerated cellulose membranes (10,000 molecular weight cut-off, Spectra/Por, USA), in the dark for 4 days then lyophilised and stored at -20 °C. HA (1.5 MDa) was also labelled with fluoresceinamine (Sigma-Aldrich) for flow cytometry analysis. Labelling (HA-FA) was performed as previously described.[39]

SAM formation and HA immobilisation:

Glass slides were cleaned with a mixture of sulphuric acid (Sigma) and 30% hydrogen peroxide (Sigma) in a 3:1 ratio, rinsed with DI water, dried under N_2 then rinsed with acetone (Sigma), dried under N_2 and finally rinsed in chloroform (Sigma) and dried under N_2. Slides were then coated with a 3 nm chromium adhesion layer, then a 100 Å layer of gold, both by evaporation. Thickness was measured by a quartz crystal oscillating monitor.

Gold coated slides were cleaned with hot (60 °C) cleaning solution (30% ammonium hydroxide (Sigma-Aldrich), 30% H_2O_2 (Sigma-Aldrich), and DI water in a 1:1:3 ratio), rinsed with DI water and dried under N_2. Surfaces were submerged in either a 1 mM ethanolic solution of peptide and incubated at room temperature overnight. For poly-D-lysine (PDL), 70 – 150 kDa (Sigma-Aldrich) coating, Au slides were cleaned, washed and dried as previously described, then incubated with 100 μg/mL PDL in dH_2O at room temperature overnight. Slides were rinsed with ethanol or dH_2O then dried under N_2. PDL was used instead of poly-L-lysine (PLL) to minimise the coatings' degradation by cells. Being made

from the artificial amino acid D-lysine, it is thought to be less susceptible to enzymatic breakdown.[29]

Samples were then incubated with a 0.5 mg/mL HA solution (molecular weight as stated) HA in dH$_2$O for at least 48 hours at room temperature. Samples were washed with dH$_2$O then dried under N$_2$ before use.

Contact Angle:

The contact angle of the bare Au, HS-Pep-1, PDL, HS-Pep-1-HA and PDL-HA (1.5 MDa) coated Au surfaces was measured by the sessile drop technique using a Drop Shape Analyser (Model DSA100, Krüss, Germany). Briefly, 1 μL of distilled water was dropped onto the surface and the contact angle was calculated using the Drop Shape Analyser inbuilt software. For each sample, the contact angle was measured at 3 different locations and the average calculated from at least 3 independent repeats.

SAM formation and HA immobilisation monitored by Quartz Crystal Microbalance with Dissipation (QCM-D):

The deposition of HA onto the HS-Pep-1, Ac-Pep-1 or PDL was monitored *in situ* by the QCM-D (Q-Sense Pro, Biolin Scientific, Sweden) in a liquid environment. Prior to that, the Au-coated 5 MHz AT-cut quartz crystal sensors (QSX301 Gold, Q-Sense, Sweden) were immersed in an oxidizing cleaning solution encompassing a 5:1:1 (v/v) mixture of ultrapure water: ammonia (25%): hydrogen peroxide (30%) in an ultrasound bath at 70 °C for 5 min. Then, the quartz crystal sensors were thoroughly rinsed with ultrapure water, dried under a gentle stream of N$_2$, and subjected to UV/ozone (UV/Ozone ProCleaner 220, BioForce Nanosciences, Inc.) treatment for 10 min. The freshly cleaned quartz crystal substrates were

then inserted in the QCM-D chamber for analysing the deposition of the various components. The quartz crystals were excited at multiple overtones (1, 3, 5, 7, 9, 11, and 13 corresponding to 5, 15, 25, 35, 45, 55, and 65 MHz, respectively) and variations in frequency (Δf) and dissipation (ΔD) were monitored in real time. The frequency of each overtone was normalized to the fundamental resonant frequency of the quartz crystal substrate ($\Delta f_n/n$; n denotes the overtone number). For all the experiments, a stable baseline was acquired with 0.15 M NaCl before the deposition of the 0.01 mM HS-Pep-1, 0.01 mM Ac-Pep-1 or 0.1 mg/mL PDL layers. The $\Delta f_n/n$ and ΔD_n were then collected as following: the quartz crystals were first equilibrated in 0.15 M NaCl for 10 minutes (baseline), following by pumping a solution of either HS-Pep-1, Ac-Pep-1, or PDL in 0.15 M NaCl into the QCM-D chamber for 10 minutes. Then, the quartz crystal sensors were rinsed with 0.15 M NaCl to remove weakly adsorbed molecules. Afterwards, a 0.5 mg/mL solution of HA (MW of either 20 kDa, 200 kDa or 1.5 MDa) or 0.5 mg/mL of alginate (low viscosity sodium alginate, Sigma-Aldrich) solution with 0.15 M NaCl was flushed into the QCM-D chamber for 10 minutes, followed by a 10 minutes rinsing step in 0.15 M NaCl, to remove loosely bounded molecules. All the experiments were performed at 25 °C and at a constant flow rate of 50 µL/min. The thickness of the PDL and HA layers was estimated using the Voigt-based viscoelastic model **(Equations 1 and 2)** implemented in the Q-Sense Dfind software (version 1.1.2672.53037), assuming a fluid PDL layer density of 1000 kg/m^3, a hydrated HA sugar density of 1050 kg/m^3, and a fluid viscosity of 1 mPa s.

$$\Delta f \approx -\frac{1}{2\pi\rho_0 h_0}\left\{\frac{\eta_3}{\delta_3} + \sum_{j=1,2}\left[h_j\rho_j\omega - 2h_j\left(\frac{\eta_3}{\delta_3}\right)^2\frac{\eta_j\omega^2}{\mu_j^2+\omega^2\eta_j^2}\right]\right\} \tag{1}$$

$$\Delta D \approx \frac{1}{2\pi f \rho_0 h_0} \left\{ \frac{\eta_3}{\delta_3} + \sum_{j=1,2} \left[2h_j \left(\frac{\eta_3}{\delta_3}\right)^2 \frac{\mu_j \omega^2}{\mu_j^2 + \omega^2 \eta_j^2} \right] \right\} \qquad (2)$$

where ρ_0 and h_0 are the density and thickness of the quartz crystal plate, η_3 is the shear viscosity of the bulk liquid, δ_3 is the viscous penetration depth of the shear wave of the bulk liquid, ρ_j and h_j are the density and thickness of the liquid overlayer, μ_j and η_j are the elastic shear modulus and shear viscosity of the liquid overlayer and ω is the angular frequency of the oscillation.

Additional estimations were also made in the case of the HS-Pep-1 layer using the Sauerbrey equation (**Equation 3**), which assumes that the added mass is rigid (negligible energy dissipation), evenly distributed over the quartz crystal sensor, and is much lower than the mass of the quartz crystal itself.

$$\Delta m = -\frac{C \times \Delta f_n}{n} \qquad (3)$$

where Δm is the Sauerbrey areal mass density of the adsorbed layers (mass per unit area), C is the mass sensitivity constant of the quartz crystal plate (17.7 ng cm^{-2} s for 5 MHz quartz crystals), n is the overtone number and Δf_n is the normalised resonant frequency.

Atomic Force Microscopy (AFM):

Samples were prepared as described above and surface topographies of the bare Au, PDL, HS-Pep-1, PDL-HA and HS-Pep-1-HA were characterised using the JPK NanoWizard 4 (JPK Instruments AG, Germany), in Quantitative Imaging mode. Silicon nitride AFM tips, MSNL-10, with a spring constant of 0.01-0.06 N/m, and a resonance frequency of 10-20 kHz were used (Bruker AFM Probes, USA). Images were taken in air and in ultra-pure water. A scan area of

10 μm x 10 μm was acquired at a resolution of 256 x 256 pixels from 3 regions of each sample. Raw images were processed by subtracting the polynomial fit from each scan line independently using the JPK Data Processing software.

Micro-Contact Printing (μCP):

PDMS stamps were prepared as previously described by Qin *et al.*[40] HS-Pep-1 was dissolved in ethanol (2 mM), swabbed onto the PDMS stamp and dried under N_2. The loaded stamp was brought into contact with base piranha cleaned gold substrate for 5 seconds. Patterned samples were then incubated with a 0.5 mg/mL solution of Texas Red-HA (1.5 MDa) in dH_2O for at least 48 hours at room temperature. Samples were rinsed twice in dH_2O then dried under N_2. Images of the μCP HS-Pep-1 SAM incubated with Texas Red-HA were then acquired using the Leica DMI4000B Epifluorescence microscope (Leica, Germany).

Detection of HA on functionalized surfaces and their interactions with serum proteins:

To demonstrate the presence of HA on the functionalized surfaces, and the ability of being recognized by hyaladherins, a fluorescent staining protocol was followed using hyaluronan binding protein (HABP) for detecting HA. This protocol has been widely used for the histochemical localization of HA in cell cultures and tissue sections.[41] To improve contrast, HS-Pep-1 patterned surfaces were first prepared by μCP as described above and using a PDMS stamp comprising an array of circular holes with 200 μm diameter. They were then incubated with a 0.5 mg/mL aqueous solution of 1.5 MDa HA for at least 48 hours at room temperature. Bare Au incubated with aqueous solution of 1.5 MDa HA (0.5 mg/mL), HS-Pep-1 patterned surfaces without or with an incubation of 0.5 mg/mL medium viscosity alginic acid sodium salt (Sigma-Aldrich) in dH2O were used as controls. Samples were rinsed with

dH2O then treated with a 5 µg/mL aqueous solution of biotinylated hyaluronic acid binding protein (composed of two binding polypeptides, derived from N-terminal regions of the hyaluronic acid binding proteoglycan and link protein, bovine nasal cartilage, Millipore) for 4 hours at room temperature. Surfaces were rinsed with dH_2O then treated with a 10 µg/mL solution of Texas red conjugated avidin (Thermo Fisher Scientific) in PBS for 2 hours at room temperature. Finally, samples were rinsed in PBS. Images were obtained at 10× and 20× magnification using Leica DMi8 Epifluorescence microscope (Leica).

The interaction of serum proteins with functionalized surfaces was monitored by QCM-D as described above. Bovine serum albumin (BSA, Sigma-Aldrich, 0.5 mg/mL in 0.15 M NaCl) or fetal bovine serum (Thermo Fisher Scientific, 10% in PBS, pH 7.4) were flowed over the various surfaces (bare Au, Pep-1 SAMs and HA immobilized on Pep-1 SAMs).

Cell Culture:

Human oral squamous cell carcinoma (SCC) derived immortalised keratinocyte CA1 and LUC4 cell lines were used for this study.[37] Cell lines were cultured in DMEM/F-12 (Gibco) and 10% (v/v) heat inactivated foetal bovine serum (FBS) (Lonza), 2 nM L-glutamine, 2% (v/v) penicillin streptomycin (PAA Laboratories) and RM+ supplement consisting of 10 ng/mL epidermal growth factor (EGF), 0.5 µg/mL hydrocortisone, 5 µg/mL insulin, 9.2×10^{-4} M liothyronine, 5 µg/mL transferrin and 1×10^{-10} M cholera toxin (Sigma). Cells were incubated at 37°c in 5% (v/v) CO_2.

Immunofluorescence:

CA1 and LUC4 cells were initially seeded on the various surfaces (Au-coated, Pep-1 SAMs and HA immobilized on Pep-1 SAMs) at a density of 10,000 cells for a 2 day experiment and

120,000 cells for 5 day experiments and cultured as described above. Bare glass slides were used as controls. Cells were washed with PBS then fixed with 4% (w/v) formaldehyde. Cells were permeablised in 0.1% (w/v) Triton X-100 (Sigma-Aldrich) then blocked in 3% (w/v) BSA (Fisher Scientific). Primary antibody (Vimentin – Dako, M0725 and Cytokeratin – Abcam, ab9377) were diluted 1:1000 in 3% (w/v) BSA and incubated overnight. Alexa 488 and Alexa 568 secondary antibodies (Invitrogen) fluorescence dye labelled secondary antibodies diluted to 1:800 in PBS was added in the following day. Cell nuclei were stained with 0.1 µg/mL of DAPI and images taken on the Leica 5000B epifluorescence microscope.

Flow cytometry analysis:

CA1 and LUC4 cells were dissociated from cell culture dishes using Accutase (Gibco). Cells were stained with CD44-FITC and EpCAM-APC (BD Pharmingen) to identify epithelial and EMT cell fractions. HA-Fluorescein (HA-FA) was also used in conjunction with EpCAM-APC. Samples were examined using Becton Dickenson LSRII machine and analysed with fluorescence activated cell sorting (FACS) Diva software (BD Biosciences).

Cell migration recorded by time-lapse microscopy:

LUC4 cells (10,000) were seeded on glass surfaces containing Au-coated stripes (1 mm width) with HA (1.5 MDa) immobilized via Pep-1 SAMs and allowed to attach for 3 hours under culture conditions described above. Cells were then imaged for 12 hours in a Zeiss Axiovert 200M time-lapse microscope.

Statistical analysis:

Quantitative data is presented as average (n=3) $\pm$ standard deviation (SD). Data from contact angle measurements and surface roughness were analysed by one-way ANOVA with

Tukey's multiple comparison to assess significant differences and data from QCM was analysed by Two-Way ANOVA.

Supporting Information
Supporting Information is available from the Wiley Online Library or from the author.

Acknowledgements

References:
[1]   a) B. P. Orner, R. Derda, R. L. Lewis, J. A. Thomson, L. L. Kiessling, *Journal of the American Chemical Society* **2004**, *126*, 10808; b) R. Derda, S. Musah, B. P. Orner, J. R. Klim, L. Y. Li, L. L. Kiessling, *Journal of the American Chemical Society* **2010**, *132*, 1289.
[2]   a) Y. Arima, H. Iwata, *Journal of Materials Chemistry* **2007**, *17*, 4079; b) D. P. Dowling, I. S. Miller, M. Ardhaoui, W. M. Gallagher, *Journal of Biomaterials Applications* **2010**, *26*, 327; c) H. Yan, S. Zhang, J. He, Y. Yin, X. Wang, X. Chen, F. Cui, Y. Li, Y. Nie, W. Tian, *Biomedical Materials* **2013**, *8*, 035008; d) B. G. Keselowsky, D. M. Collard, A. J. García, *Proceedings of the National Academy of Sciences* **2005**, *102*, 5953; e) B. Valamehr, S. J. Jonas, J. Polleux, R. Qiao, S. Guo, E. H. Gschweng, B. Stiles, K. Kam, T.-J. M. Luo, O. N. Witte, X. Liu, B. Dunn, H. Wu, *Proceedings of the National Academy of Sciences* **2008**, *105*, 14459.
[3]   B. G. Keselowsky, D. M. Collard, A. J. García, *Journal of Biomedical Materials Research Part A* **2003**, *66A*, 247.
[4]   V. Corvaglia, R. Marega, F. De Leo, C. Michiels, D. Bonifazi, *Small* **2016**, *12*, 321.
[5]   a) C. Roberts, C. S. Chen, M. Mrksich, V. Martichonok, D. E. Ingber, G. M. Whitesides, *Journal of the American Chemical Society* **1998**, *120*, 6548; b) C. S. Chen, M. Mrksich,

S. Huang, G. M. Whitesides, D. E. Ingber, *Biotechnology Progress* **1998**, *14*, 356.

[6] a) H. Kim, H. Jeong, S. Han, S. Beack, B. W. Hwang, M. Shin, S. S. Oh, S. K. Hahn, *Biomaterials* **2017**, *123*, 155; b) K. Meyer, J. W. Palmer, *Journal of Biological Chemistry* **1934**, *107*, 629.

[7] B. P. Toole, *Nature Reviews Cancer* **2004**, *4*, 528.

[8] Z. Zhang, G. F. Christopher, *Soft Matter* **2015**, *11*, 2596.

[9] A. F. Silva, M. A. Alves, M. S. N. Oliveira, *Rheologica Acta* **2017**, *56*, 377.

[10] a) W. Knudson, C. Biswas, X. Q. Li, R. E. Nemec, B. P. Toole, *Ciba Found Symp* **1989**, *143*, 150; b) M. G. Slomiany, L. Dai, P. A. Bomar, T. J. Knackstedt, D. A. Kranc, L. Tolliver, B. L. Maria, B. P. Toole, *Cancer Research* **2009**, *69*, 4992; c) E. A. Turley, P. W. Noble, L. Y. W. Bourguignon, *Journal of Biological Chemistry* **2002**, *277*, 4589; d) L. Collis, C. Hall, L. Lange, M. Ziebell, R. Prestwich, E. A. Turley, *FEBS Letters* **1998**, *440*, 444; e) B. P. Toole, M. G. Slomiany, *Drug Resistance Updates* **2008**, *11*, 110.

[11] M. E. Prince, R. Sivanandan, A. Kaczorowski, G. T. Wolf, M. J. Kaplan, P. Dalerba, I. L. Weissman, M. F. Clarke, L. E. Ailles, *Proceedings of the National Academy of Sciences* **2007**, *104*, 973.

[12] S. I. Sayed, R. C. Dwivedi, R. Katna, A. Garg, K. A. Pathak, C. M. Nutting, P. Rhys-Evans, K. J. Harrington, R. Kazi, *Oral Oncology* **2011**, *47*, 237.

[13] a) L. Y. W. Bourguignon, G. Wong, C. Earle, L. Chen, *Journal of Biological Chemistry* **2012**, *287*, 32800; b) L. Y. W. Bourguignon, G. Wong, M. Shiina, *Journal of Biological Chemistry* **2016**, *291*, 10571.

[14] F. Bano, S. Banerji, M. Howarth, D. G. Jackson, R. P. Richter, *Scientific reports* **2016**, *6*, 34176.

[15] a) E. Lih, S. G. Choi, D. J. Ahn, Y. K. Joung, D. K. Han, *Journal of tissue engineering* **2016**, *7*, 2041731416683745; b) R. Huang, X. Liu, H. Ye, R. Su, W. Qi, L. Wang, Z. He, *Langmuir* **2015**, *31*, 12061.

[16] B. B. Minsky, C. H. Antoni, H. Boehm, *Scientific reports* **2016**, *6*, 21608.

[17] M. S. Lord, D. Pasqui, R. Barbucci, B. K. Milthorpe, *Journal of Biomedical Materials Research Part A* **2009**, *91A*, 635.

[18] a) X. Liu, R. Huang, R. Su, W. Qi, L. Wang, Z. He, *ACS Applied Materials & Interfaces* **2014**, *6*, 13034; b) M. Ombelli, L. Costello, C. Postle, V. Anantharaman, Q. C. Meng, R. J. Composto, D. M. Eckmann, *Biofouling* **2011**, *27*, 505; c) J.-H. Choi, S.-O. Kim, E. Linardy, E. C. Dreaden, V. P. Zhdanov, P. T. Hammond, N.-J. Cho, *Journal of Colloid and Interface Science* **2015**, *448*, 197; d) M. A. J. Mazumder, *Arabian Journal for Science and Engineering* **2017**, *42*, 271.

[19] G. Chen, Y. Ito, Y. Imanishi, A. Magnani, S. Lamponi, R. Barbucci, *Bioconjugate Chemistry* **1997**, *8*, 730.

[20] C. F. Wertz, M. M. Santore, *Langmuir* **1999**, *15*, 8884.

[21] M. E. Mummert, M. Mohamadzadeh, D. I. Mummert, N. Mizumoto, A. Takashima, *The Journal of experimental medicine* **2000**, *192*, 769.

[22] I. M. Martins, R. L. Reis, H. S. Azevedo, *ACS Chemical Biology* **2016**, *11*, 2962.

[23] a) S. R. Rudrabhatla, C. L. Mahaffey, M. E. Mummert, *Journal of Investigative Dermatology* **2006**, *126*, 1378; b) J. M. Zmolik, M. E. Mummert, *Journal of Histochemistry & Cytochemistry* **2005**, *53*, 745.

[24] a) M. E. Mummert, D. I. Mummert, L. Ellinger, A. Takashima, *Molecular Cancer Therapeutics* **2003**, *2*, 295; b) M. E. Mummert, D. Mummert, D. Edelbaum, F. Hui, H. Matsue, A. Takashima, *The Journal of Immunology* **2002**, *169*, 4322.

[25]   a) A. Singh, P. Li, V. Beachley, P. McDonnell, J. H. Elisseeff, *Contact Lens and Anterior Eye* **2015**, *38*, 79; b) A. Singh, M. Corvelli, S. A. Unterman, K. A. Wepasnick, P. McDonnell, J. H. Elisseeff, *Nature materials* **2014**, *13*, 988.

[26]   a) K. A. Marx, *Biomacromolecules* **2003**, *4*, 1099; b) C. Picart, P. Lavalle, P. Hubert, F. J. G. Cuisinier, G. Decher, P. Schaaf, J. C. Voegel, *Langmuir* **2001**, *17*, 7414.

[27]   M. A. Díez-Pascual, S. P. Shuttleworth, *Materials* **2014**, *7*.

[28]   M. S. Niepel, F. Almouhanna, B. K. Ekambaram, M. Menzel, A. Heilmann, T. Groth, *The International Journal of Artificial Organs* **2018**, *41*, 223.

[29]   W.-C. Shen, H. J. P. Ryser, *Molecular Pharmacology* **1979**, *16*, 614.

[30]   a) A. Schmaus, S. Klusmeier, M. Rothley, A. Dimmler, B. Sipos, G. Faller, W. Thiele, H. Allgayer, P. Hohenberger, S. Post, J. P. Sleeman, *British journal of cancer* **2014**, *111*, 559; b) R. Stern, *European Journal of Cell Biology* **2004**, *83*, 317; c) C. C. Termeer, J. Hennies, U. Voith, T. Ahrens, J. M. Weiss, P. Prehm, J. C. Simon, *The Journal of Immunology* **2000**, *165*, 1863.

[31]   D. Johannsmann, *Physical Chemistry Chemical Physics* **2008**, *10*, 4516.

[32]   M. Rodahl, B. Kasemo, *Review of Scientific Instruments* **1996**, *67*, 3238.

[33]   S. Amorim, D. S. da Costa, D. Freitas, C. A. Reis, R. L. Reis, I. Pashkuleva, R. A. Pires, *Scientific Reports* **2018**, *8*, 16058.

[34]   M. Van Beek, L. Jones, H. Sheardown, *Biomaterials* **2008**, *29*, 780.

[35]   a) J. Liang, D. Jiang, P. W. Noble, *Advanced Drug Delivery Reviews* **2016**, *97*, 186; b) S. J. Wang, V. B. Wreesmann, L. Y. Bourguignon, *Head Neck* **2007**, *29*, 550.

[36]   L. E. Dickinson, C. C. Ho, G. M. Wang, K. J. Stebe, S. Gerecht, *Biomaterials* **2010**, *31*, 5472.

[37]   A. Biddle, X. Liang, L. Gammon, B. Fazil, L. J. Harper, H. Emich, D. E. Costea, I. C. Mackenzie, *Cancer Research* **2011**, *71*, 5317.

[38]   S. Ribeiro, E. Radvar, Y. Shi, J. Borges, R. P. Pirraco, I. B. Leonor, J. F. Mano, R. L. Reis, Á. Mata, H. S. Azevedo, *Nanoscale* **2017**, *9*, 13670.

[39]   D. S. Ferreira, A. P. Marques, R. L. Reis, H. S. Azevedo, *Biomaterials Science* **2013**, *1*, 952.

[40]   D. Qin, Y. N. Xia, G. M. Whitesides, *Nature Protocols* **2010**, *5*, 491.

[41]   C. A. de la Motte, J. A. Drazba, *The journal of histochemistry and cytochemistry : official journal of the Histochemistry Society* **2011**, *59*, 252.

Table 1: **Average changes in $\Delta f_7/7$ (Hz) and ΔD_7 at the equilibrium, as measured by QCM-D, and modelled thickness (h, nm) and areal mass density (Δm, ng/cm^2),** derived using the Sauerbrey equation and the Voigt-based viscoelastic model. All values are the average of 3 independent experiments ± SD. (†Average of 2 independent experiments.)

	$\Delta f_7/7$ (Hz)	ΔD_7 (x10^{-6})	Voigt Thickness, h_{Voigt} (nm)	Voigt Mass Density, Δm_{Voigt} (ng/cm^2)	Sauerbrey Thickness, $h_{Sauerbrey}$ (nm)	Sauerbrey Mass density, $\Delta m_{Sauerbrey}$ (ng/cm^2)
Adsorption onto Au						
HS-Pep-1	-18.7±1.2	0.3±0.3	3.7±1.0	354.1±96.6	3.3±0.6	329.6±65.5
PDL	-12.4±1.5	0.7±0.3	12.9±3.6	1276.0±366.4	-	-
Adsorption onto HS-Pep-1						
1.5 MDa HA	-9.1±2.7	1.8±0.2	10.8±4.8	1154.0±492.1	-	-
200 kDA HA	-9.7±2.5	1.4±0.4	10.4±1.4	919.5±329.5	-	-
20 kDa HA	-5.5±1.1	0.6±0.2	5.4±1.8	640.0±147.3	-	-
Adsorption onto PDL						
1.5 MDa HA	-16.1±0.3	2.4±0.3	12.1±6.6	1342.0±653.7	-	-
200 kDA HA	-11.5±1.6	1.5±0.4	3.8±1.5	396.7±166.2	-	-
20 kDa HA†	-9.7±0.4	0.5±0.1	1.6±0.4	270.0±99.0	-	-
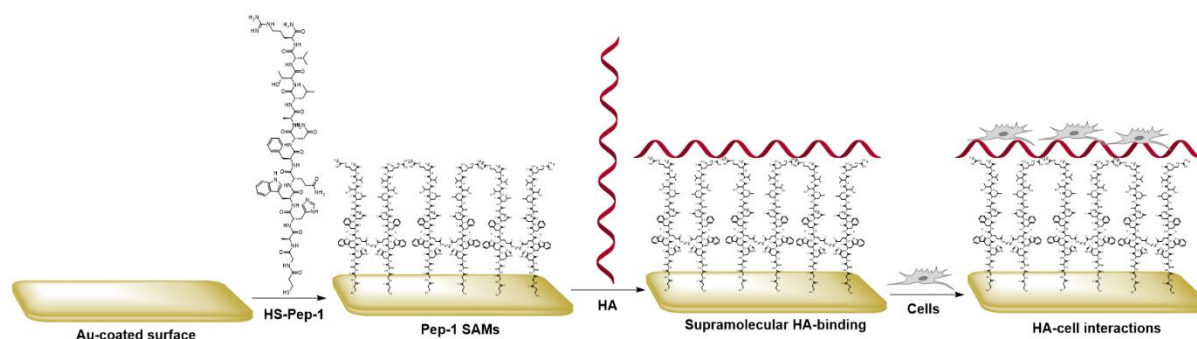
Scheme 1: **Schematic illustration of the proposed supramolecular immobilisation of HA on surfaces to study cell behaviour.**

.
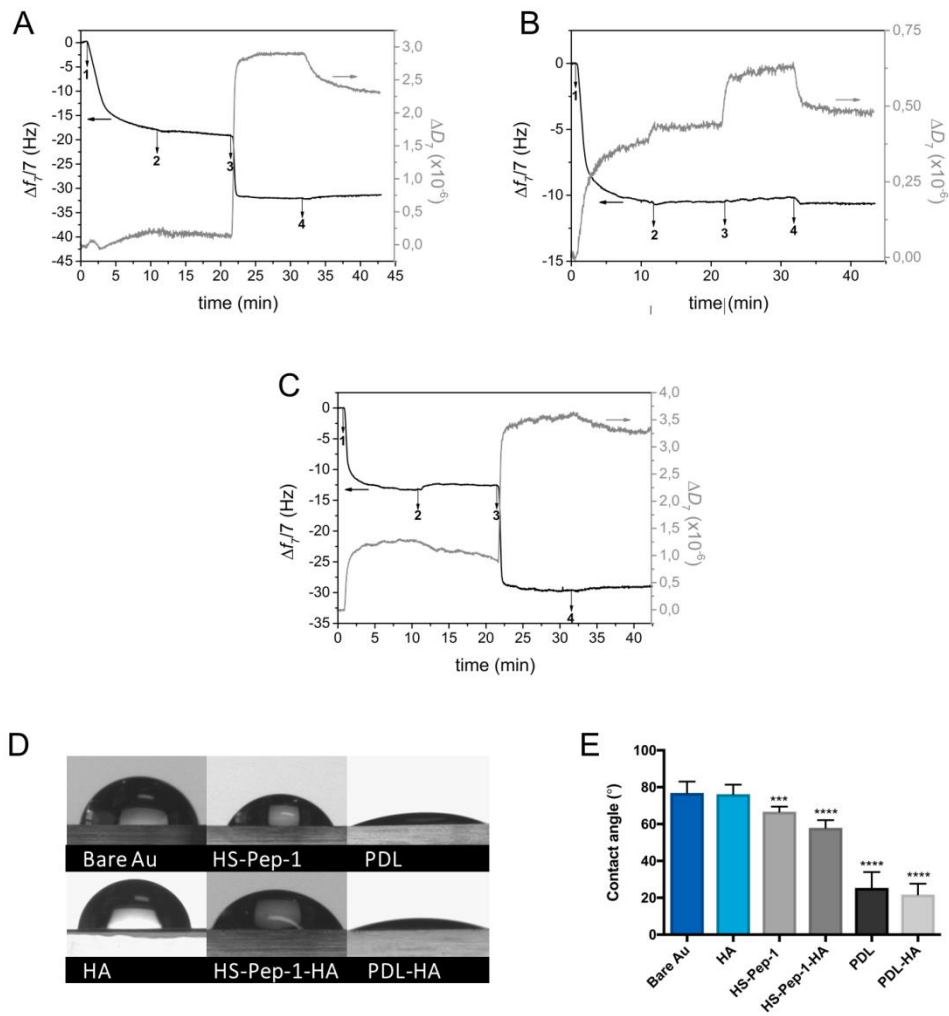
Figure 1: **HS-Pep-1 attaches to an Au substrate which can then bind HA.** Representative QCM-D data showing the normalised frequency ($\Delta f_n/n$) and dissipation (ΔD_n) shifts obtained at the 7th overtone ($n = 7$; 35 MHz) as a function of time for the deposition of HA onto HS-Pep-1 (A), Ac-Pep-1 (B), or PDL (C) modified Au-coated quartz crystal sensors with intermediate rinsing steps. Numbers refer to the adsorption of HS-Pep-1, Ac-Pep-1, or PDL (1), 1.5 MDa HA (3), and rinsing steps (2, and 4). The addition of a 0.01 mM HS-Pep-1, 0.01 mM Ac-Pep-1, or 0.1 mg/mL PDL in 150 mM NaCl (1) leads to a decrease in the frequency shift which is maintained upon washing (2). The addition of 1.5 MDa HA in 150 mM NaCl (3) to HS-Pep-1 or PDL-coated crystals causes a further decrease in frequency shift (A and C). The addition of 1.5 MDa HA in 150 mM NaCl (3) to Ac-Pep-1 coated crystals did not alter the

frequency shift (B). Water contact angle images of the prepared surfaces (D) and a graph showing the average contact angles for all surfaces (E). n=3, error = SD, ****= $p<0.0001$, ***=$p<0.001$ compared to bare Au control (one-way ANOVA with Tukey's multiple comparison).
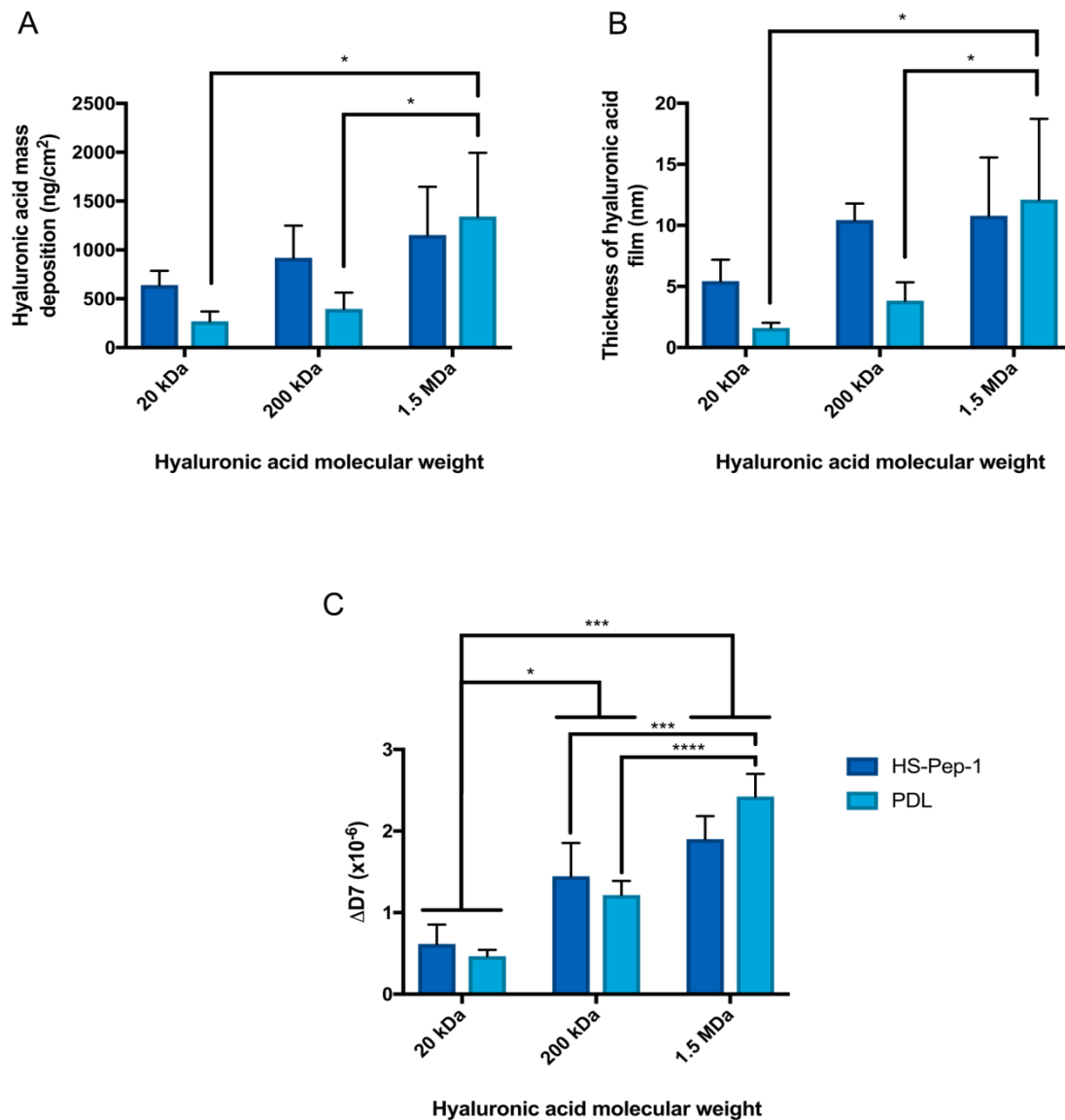
Figure 2: **Molecular weight of hyaluronic acid has minimal impact on its deposition on HS-Pep-1 and PDL coated surfaces.** Bar graph showing the average areal mass density (A) and hydrodynamic thickness (B) of HA deposited onto either a HS-Pep-1 or PDL surface calculated using the Voigt-based viscoelastic model. Bar graph showing the change in the

dissipation factor at the 7th overtone upon HA binding to HS-Pep-1 or PDL surfaces following washing as measured by QCM-D (C). n=3, error = SD, ****=p<0.0001 ***= p<0.0002, *= p<0.0332 (Two-Way ANOVA).
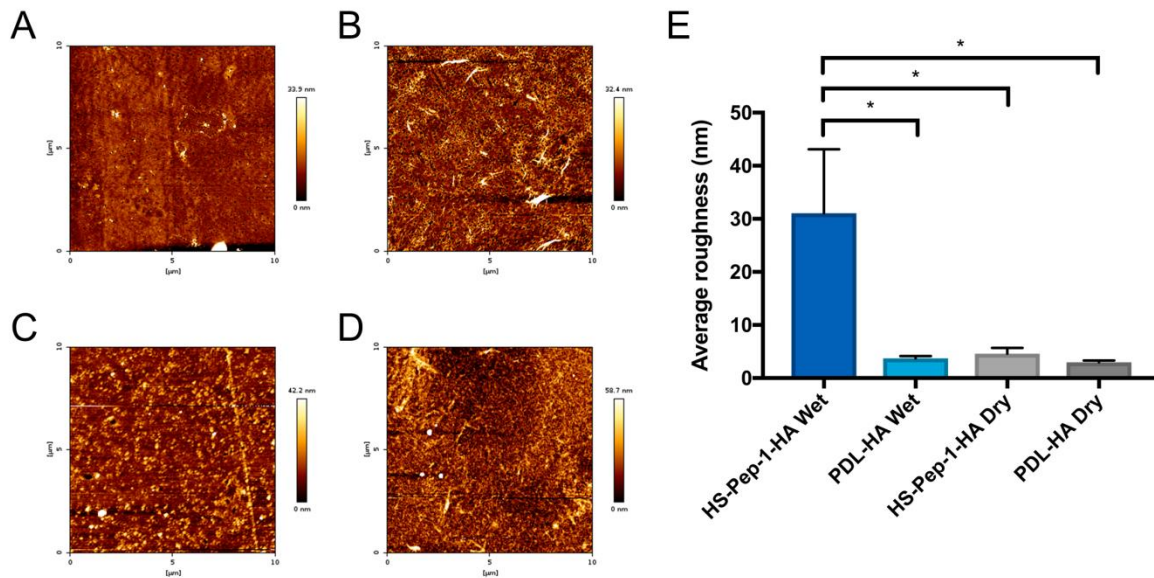
Figure 3: **Immobilisation of HA (1.5 MDa) by PDL and HS-Pep-1 produces substrates with different topographies.** Representative AFM topographic images (10×10 μm^2) of PDL-HA (A, C) and HS-Pep-1-HA (B, D) layers in dried (A, B) and hydrated (C, D) states, respectively. Bar graph showing the mean average roughness of HS-Pep-1-HA and PDL-HA samples under dry or hydrated conditions (E). n=3, error = SEM, * = $p < 0.0332$, (one-way ANOVA with Tukey's multiple comparisons).
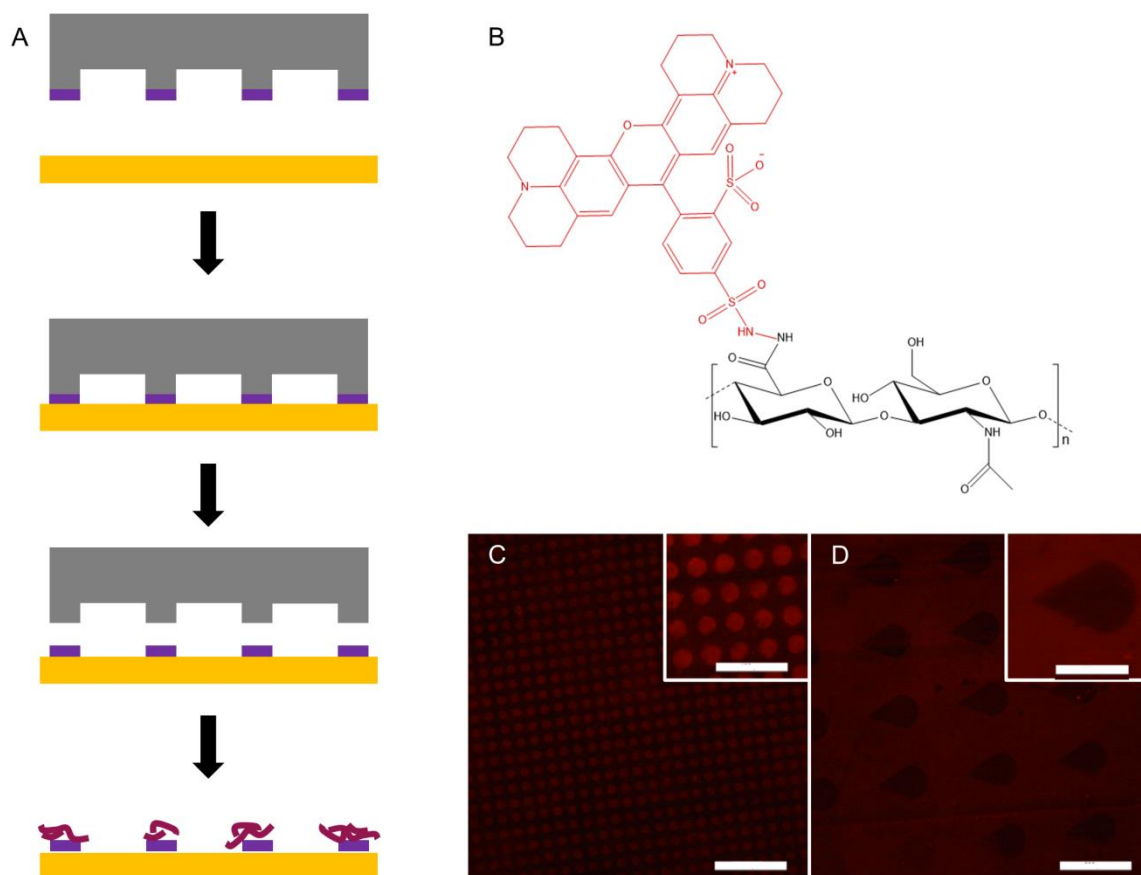
Figure 4: **HS-Pep-1-HA patterning of surfaces using μ-contact printing.** Schematic illustration of the PDMS stamp (grey) loaded with peptide (purple), which is transferred to the gold surface on contact. The peptide is then able to immobilise HA (red) (A). Chemical structure of the Texas Red-labelled HA (B). Fluorescence images of surfaces patterned with a HS-Pep-1-coated PDMS stamp then incubated with Texas Red-labelled 1.5 MDa HA, creating a spot pattern where HA is deposited in distinct foci (C) or a 'negative' drop pattern where HA forms a background coating (D). Scale bar = 200 μm on the large images and 100 μm on the inserts.
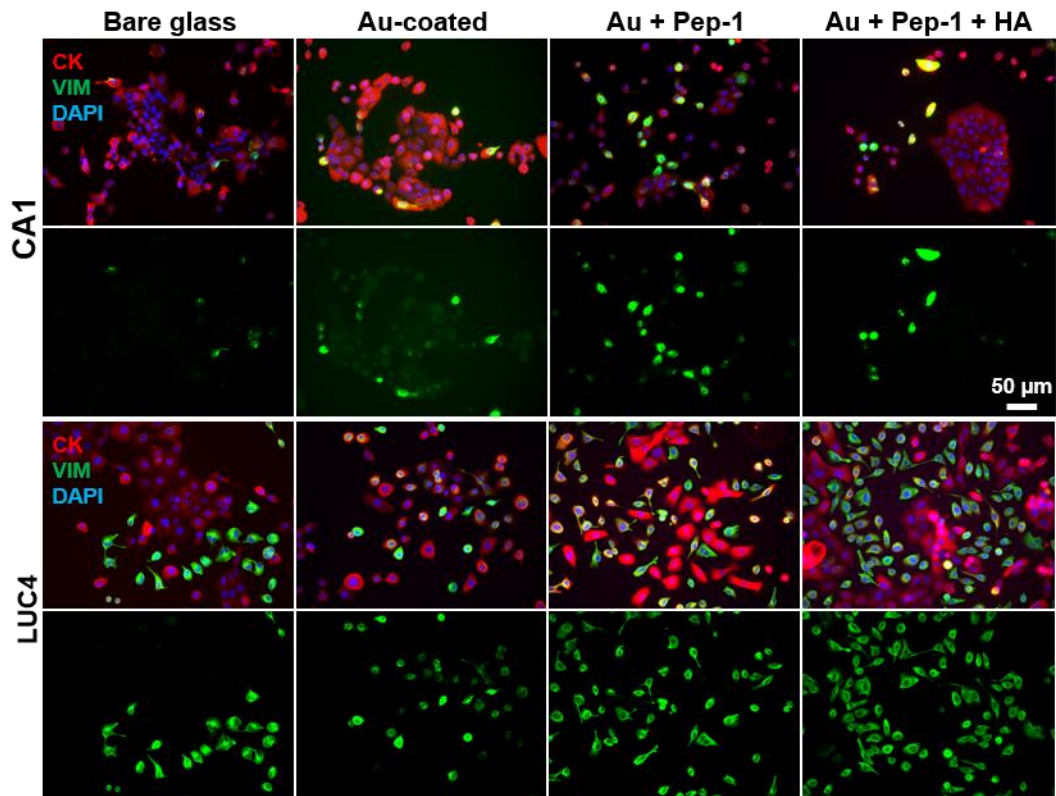
Figure 5: **Increased number of EMT cells bind to HA functionalized surfaces.** Fluorescence microscopy images of CA1 and LUC4 cells cultured on the various surfaces for 5 days and stained with vimentin (VIM) and cytokeratin (CK) which are positive markers for EMT and epithelial cells, respectively. Scale bar is the same for all images.
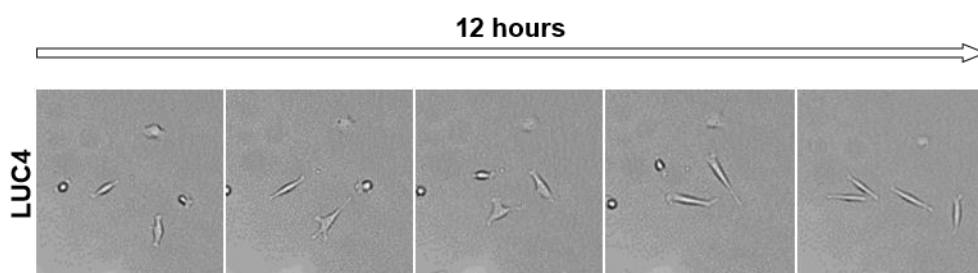
Figure 6: **LUC4 cells adhere to HA immobilized on surfaces, remain attached and displayed constant shifting to and from an EMT phenotype.** Snapshots from time-lapse imaging showing the morphology of LUC4 cells attached on HA (1.5 MDa) immobilized on Au stripes coated on glass slides via Pep-1 SAMs.

The use of a peptide-based SAM allows the supramolecular presentation of unmodified hyaluronan (HA) for *in vitro* cell culture. Micro-contact printing of the peptide permits the formation of patterned HA surfaces for more complex *in vitro* cell culture studies. The surfaces generated using this platform are used to study the behavior of cancer stem cells on immobilized HA.

Keyword: Hyaluronan, self-assembled monolayers, peptides, cancer stem cells, model surfaces

X. Pang, C. O'Malley, J. Borges, M. M. Rahman, D. W. P. Collis, J. F. Mano, I. Mackenzie, H. S.

Azevedo*

Title Supramolecular Presentation of Hyaluronan onto Model Surfaces for Studying the Behaviour of Cancer Stem Cells

ToC figure
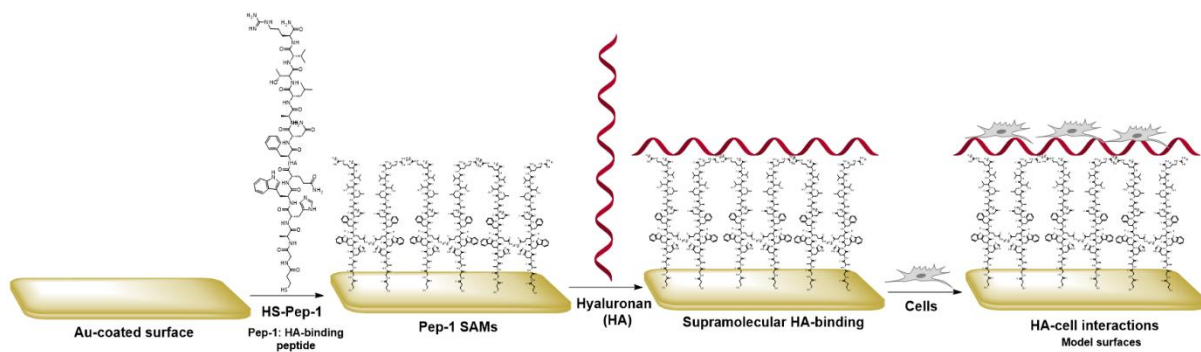
Supporting Information

Supramolecular Presentation of Hyaluronan onto Model Surfaces for Studying the Behaviour of Cancer Stem Cells

Xinqing Pang, Clare O'Malley, João Borges, Muhammad M. Rahman, Dominic W. P. Collis,

João F. Mano, Ian C. Mackenzie, and Helena S. Azevedo*
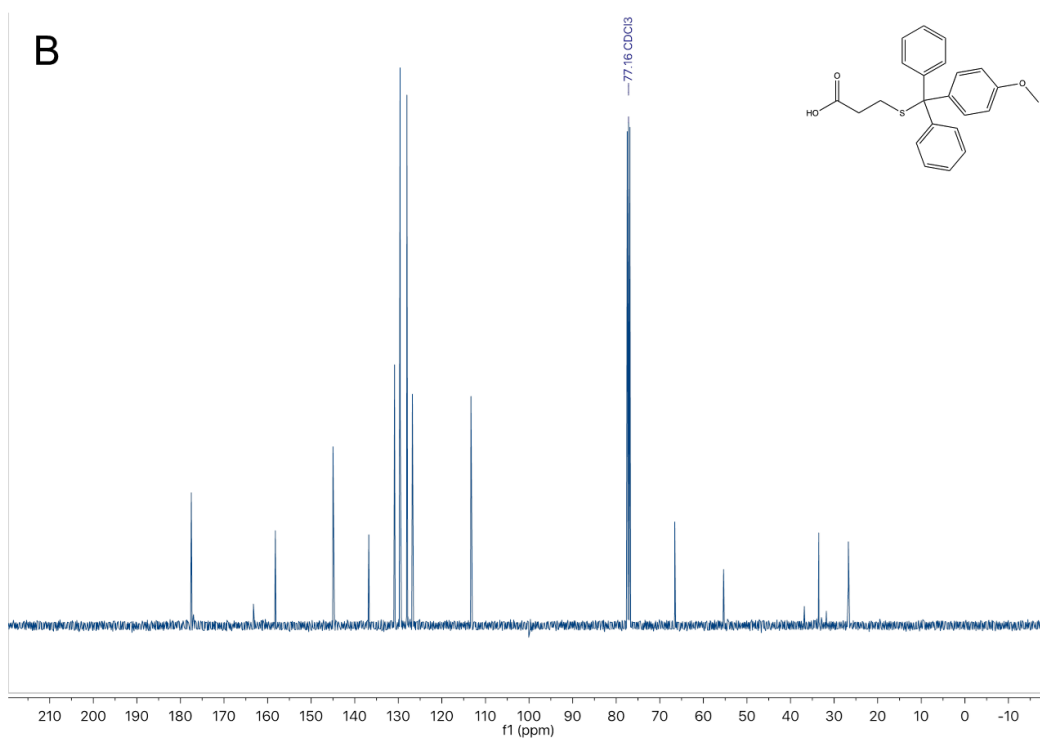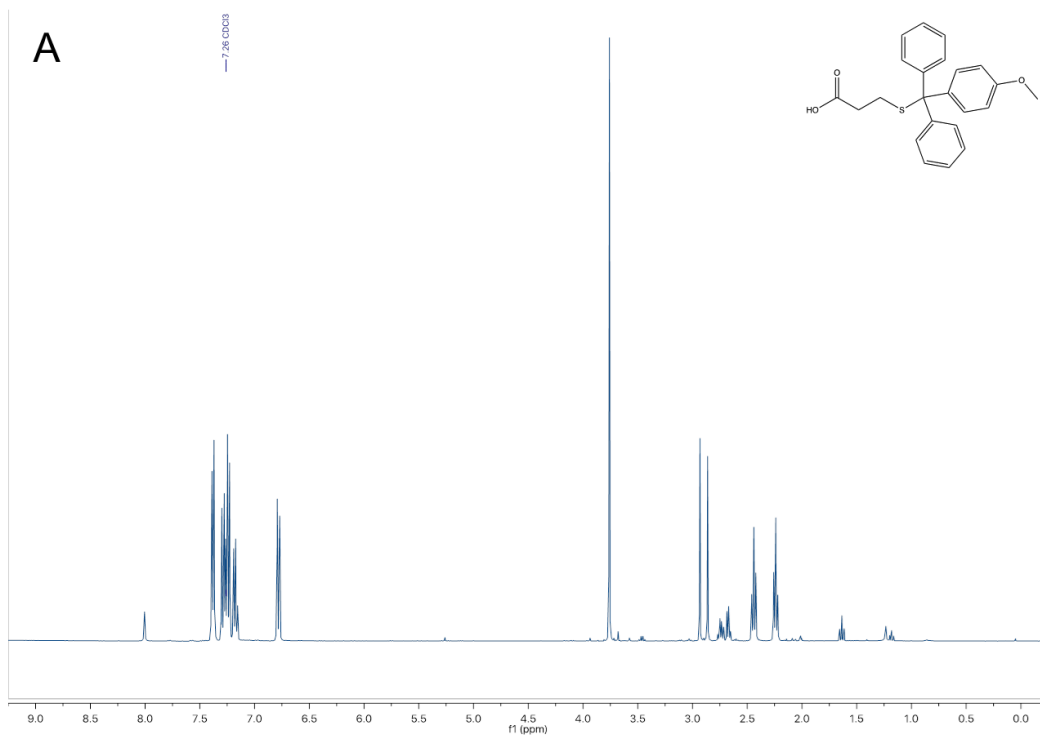
Figure S1: NMR analysis of 3-(((4-methoxyphenyl)diphenylmethyl)thio) propanoic acid. ^{1}H **NMR** (400 MHz, CDCl$_3$) δ (ppm) = 7.44 (d, 7.2 Hz, 4H, *o*-CH), 7.35 (d, 9.0 Hz, 2H, *o*-CH), 7.29 (t, 5.8 Hz, 4H, *m*-CH), 7.24 - 7.18 (t, 2H, *p*-CH), 6.80 (d, 9.0 Hz, 2H, *m*-CH), 3.78 (s, 3H, CH$_3$),

2.49 (t, 7.5 Hz, 2H, SCH₂), 2.28 (t, 7.5 Hz, 2H, CH$_2$COOH) (A). ^{13}C NMR (101 MHz, CDCl$_3$) δ (ppm) = 177.52 (**C**OOH), 158.23 (**C**OCH$_3$), 145.00 (C**C** phenyl ring), 136.78 (C**C**H, PhOCH$_3$), 130.87 (ortho-**C**H, PhOCH$_3$), 129.58 (meta-**C**H, phenyl ring), 128.04 (ortho-**C**H, phenyl ring), 126.79 (meta-**C**H, phenyl ring), 113.32 (meta-**C**H, PhOCH$_3$), 66.56 (**C**(PhOCH$_3$)Ph$_2$), 55.35 (O**C**H$_3$), 33.53(HOOC**C**H$_2$), 26.72 (CH$_2$**C**H$_2$C) (B).

A

B
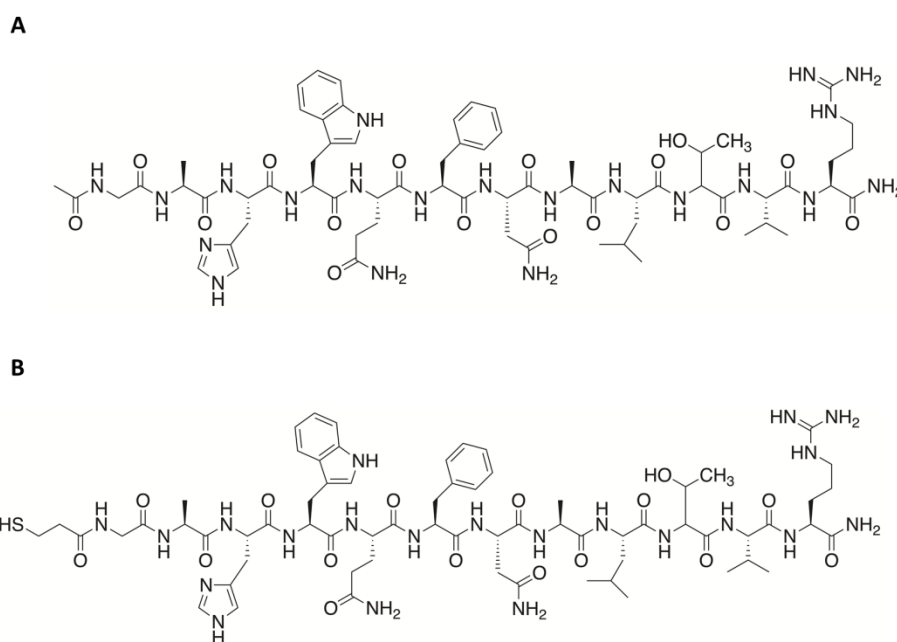
Figure S2: **Chemical structure of peptides used in this study.** Acetylated Pep-1 (A) and thiolated Pep-1 (B) drawn in Chemdraw Prime 17.1.
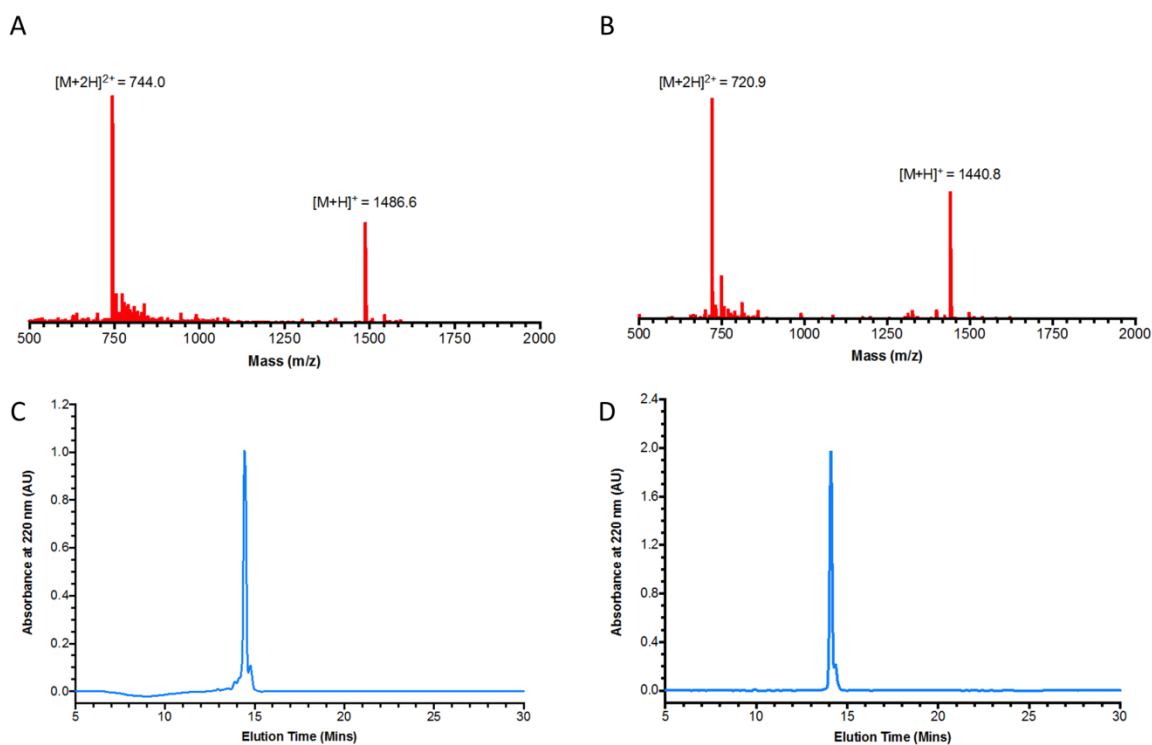
Figure S3: **Characterisation of synthesised peptides.** Electrospray Ionisation Mass Spectrometry of (A) HS-Pep-1-CONH$_2$ (Found 1486.6 [M+H]$^+$, 744.0 [M+2H]$^{2+}$. Expected 1486.7) and (B) Ac-Pep-1-CONH$_2$ (Found 1440.8 [M+H]$^+$, 720.9 [M+2H]$^{2+}$. Expected 1440.6) High Performance Liquid Chromatography trace of (C) HS-Pep-1-CONH$_2$ and (D) Ac-Pep-1-CONH$_2$ showing a single peak.
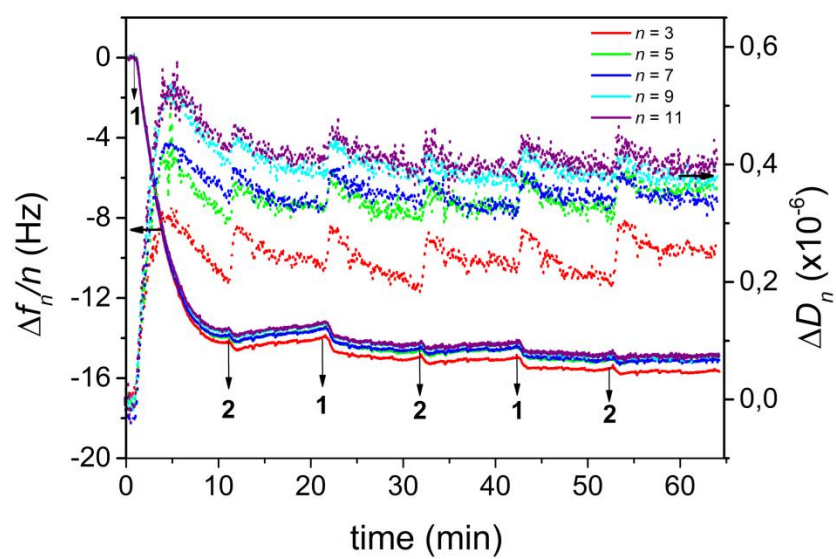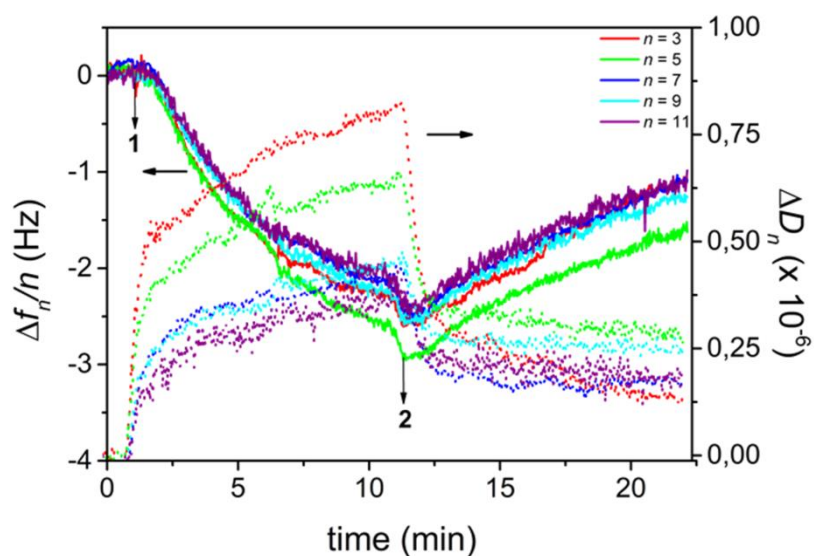
Figure S4: **Representative QCM-D data for the normalised frequency (Δf_n/n) and dissipation (ΔD_n) shifts** obtained as a function of time for the deposition of HS-Pep-1 (1) onto Au-coated quartz crystal sensors and rinsing step (2).
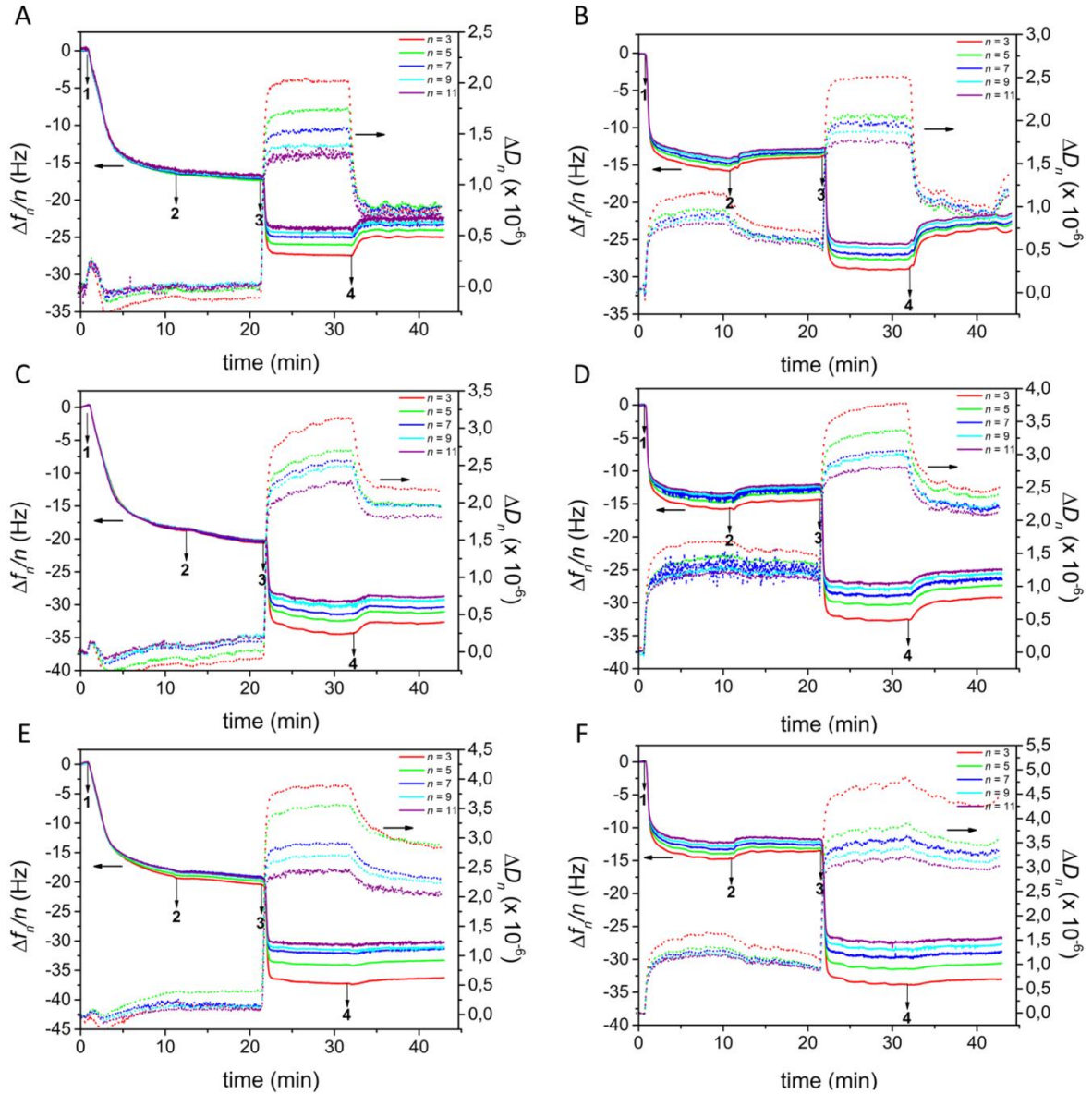
Figure S5: **QCM-D measurement of the normalised frequency ($\Delta f_n/n$) and dissipation (ΔD_n) shifts** with a range of HA molecular weights. Representative QCM-D data for $\Delta f_n/n$ and ΔD_n as a function of time for the deposition of HA onto HS-Pep-1- and PDL-modified Au-coated quartz crystal sensors and rinsing steps. Numbers refer to the adsorption of (1) HS-Pep-1 (A, C, E) or PDL (B, D, F), (2) rinsing step, the adsorption of (3) 20 kDa HA (A, B), 200 kDa (C, D) or 1.5 MDa HA (E, F) and a further (4) rinsing step. For both HS-Pep-1 and PDL their addition in an aqueous solution of 150 mM NaCl leads to a decrease in frequency shift which is maintained on washing. A further decrease in frequency shift was seen on addition of each HA molecular weight, which was also maintained on washing.

Figure S6: **Representative QCM-D data for the normalised frequency (Δf_n/n) and dissipation (ΔD_n) shifts** as a function of time for the deposition of 200 kDa HA on Au-coated quartz crystal sensors and rinsing steps. Numbers refer to the adsorption of (1) HA and (2) rinsing step. The addition of HA aqueous solution in 150 mM NaCl leads to a decrease in frequency shift which is reversed on washing. This result shows negligible HA adsorption onto the Au-coated quartz crystal.
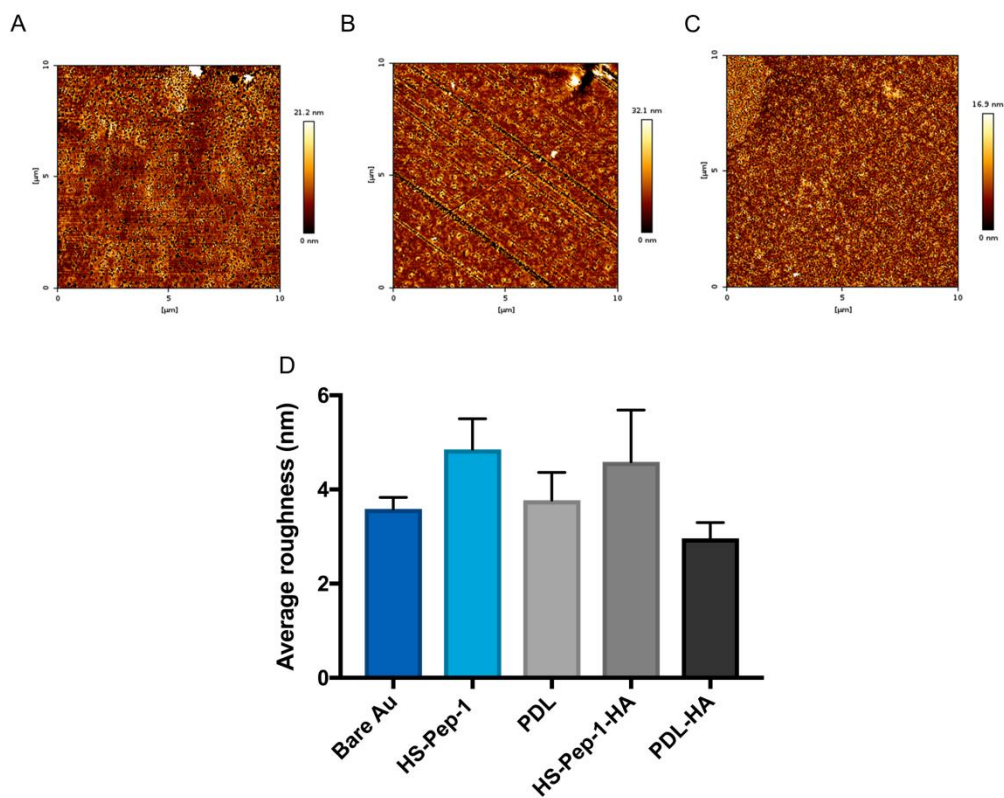
Figure S7: **AFM analysis of uncoated and coated Au surfaces.** Representative AFM topographic images (10 × 10 μm^2) of bare Au (A), HS-Pep-1-coated Au (B) and PDL-coated Au (C) in air. Bar graph showing the mean average roughness of bare Au, HS-Pep-1, PDL, HS-Pep-1-HA, and PDL-HA surfaces in a dried state (D). n=3, error = SD.
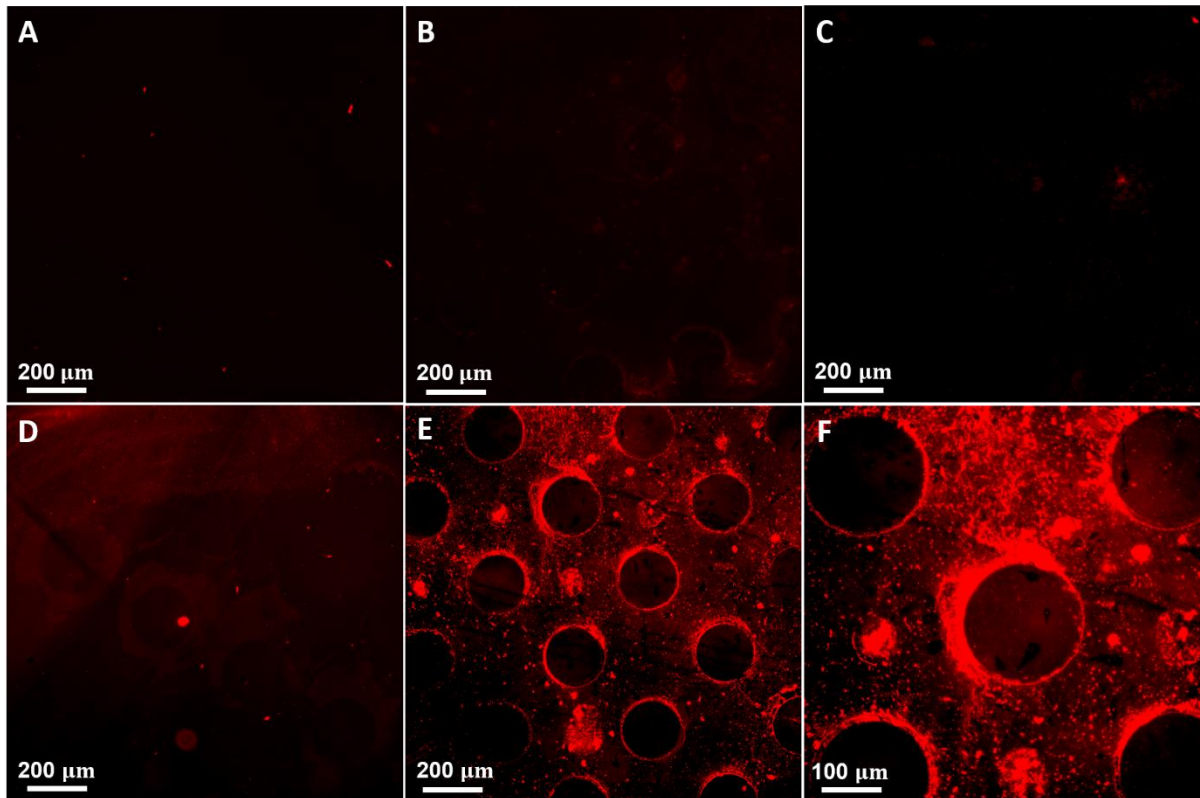
Figure S8: **Detection of HA on functionalized surfaces with hyaluronan binding protein (HABP)**. Fluorescence microscopy images of surfaces after incubation with biotinylated HABP followed by avidin-Texas red. (A) HA (1.5 MDa, 0.5 mg/mL) on bare Au; (B) patterned Pep-1 SAMs on Au; (C) alginate over patterned Pep-1 SAMs on Au; (D) HA (1.5 MDa, 0.5 mg/mL) on PDL patterns; (E) HA (1.5 MDa, 0.5 mg/mL) over patterned Pep-1 SAMs on Au; (F) is a magnification of (E). The staining shows the presence of HA only on surfaces where HA was immobilized via Pep-1 SAMs (E).
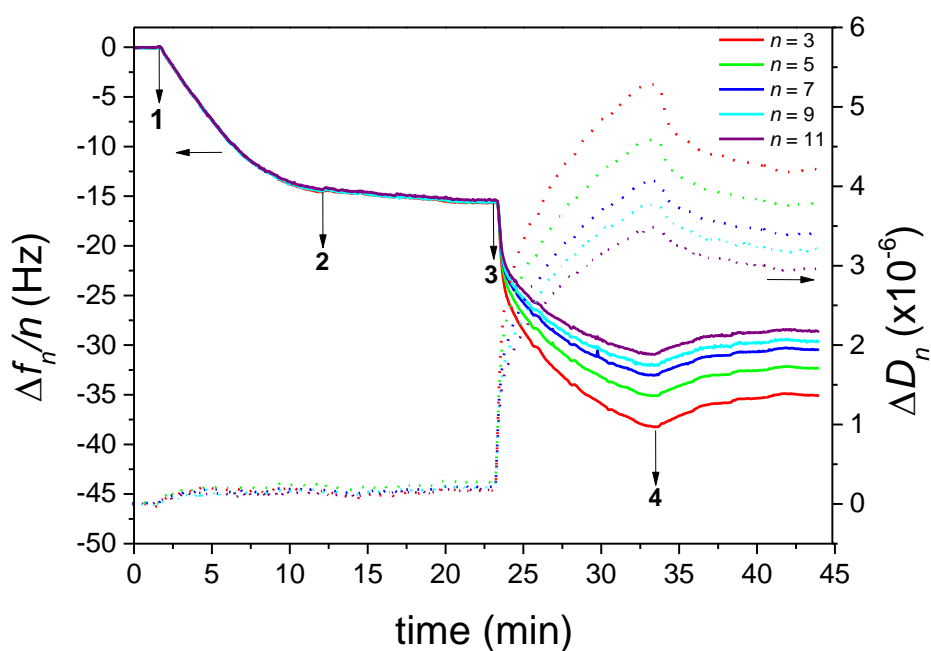
Figure S9: **Representative QCM-D data for the normalised frequency ($\Delta f_n/n$) and dissipation (ΔD_n) shifts** for the adsorption of alginate onto the HS-Pep-1-modified Au substrate. Numbers refer to (1) adsorption of HS-Pep-1, (2) rinsing step, (3) adsorption of alginate, (4) rinsing step. A decrease in the frequency shift was seen on the addition of alginate, which was slightly removed on washing.
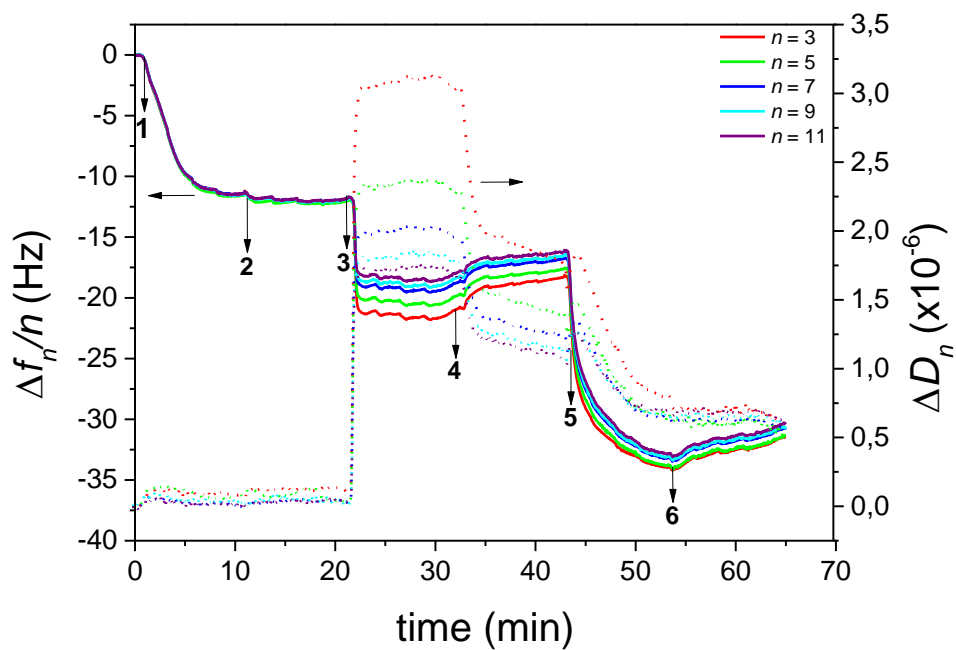
Figure S10: **Representative QCM-D data for the normalised frequency (Δf$_n$/n) and dissipation (ΔD$_n$) shifts** for the adsorption of BSA (0.05%) over the HA layer immobilized on the Pep-1 SAMs. Numbers refer to (1) adsorption of HS-Pep-1, (2) rinsing step, (3) deposition of HA, (4) rinsing step, (5) adsorption of BSA, (6) rinsing step. A decrease in frequency shift was seen upon the addition of BSA, which was slightly removed on washing.
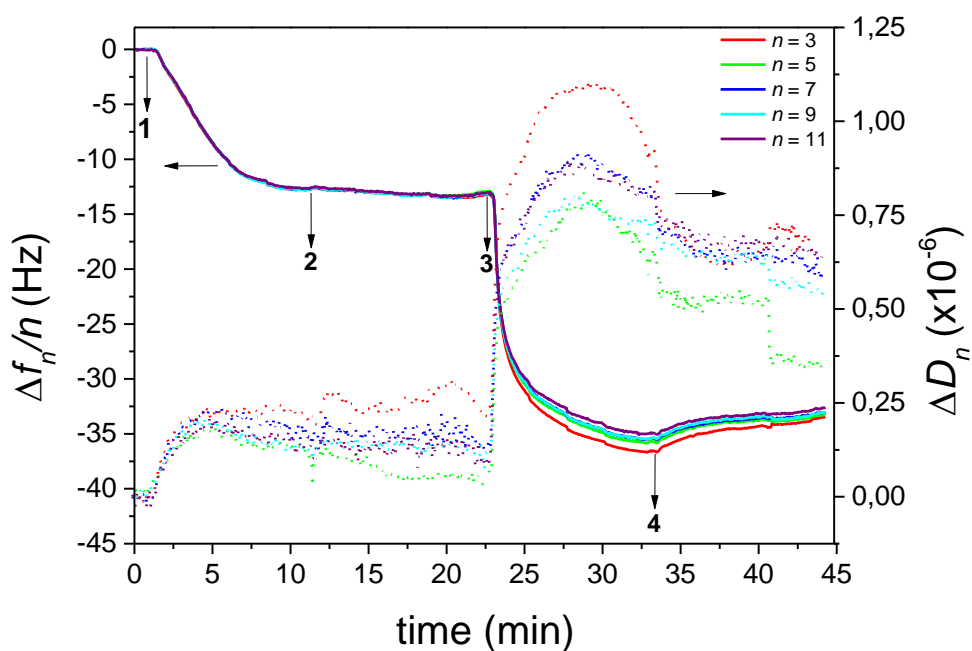
Figure S11: **Representative QCM-D data for the normalised frequency (Δf$_n$/n) and dissipation (ΔD$_n$) shifts** for the adsorption of BSA (0.05%) over the HS-Pep-1 functionalized Au substrate. Numbers refer to (1) adsorption of Pep-1, (2) rinsing step, (3) adsorption of BSA, (4) rinsing step. A decrease in frequency shift was seen upon addition of BSA, which was maintained upon washing.
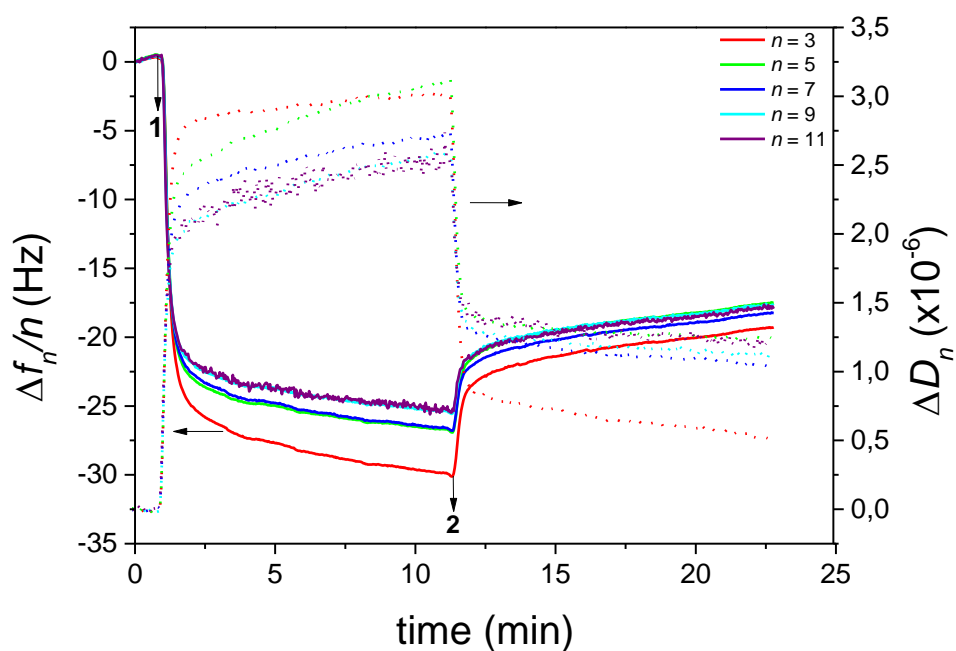
Figure S12: **Representative QCM-D data for the normalised frequency (Δf$_n$/n) and dissipation (ΔD$_n$) shifts** for the adsorption of FBS (10%) onto the bare Au substrate. Numbers refer to (1) adsorption of FBS, (2) rinsing step. The addition of FBS in PBS solution (pH 7.4) led to a decrease in frequency shift, which was partially removed upon washing.
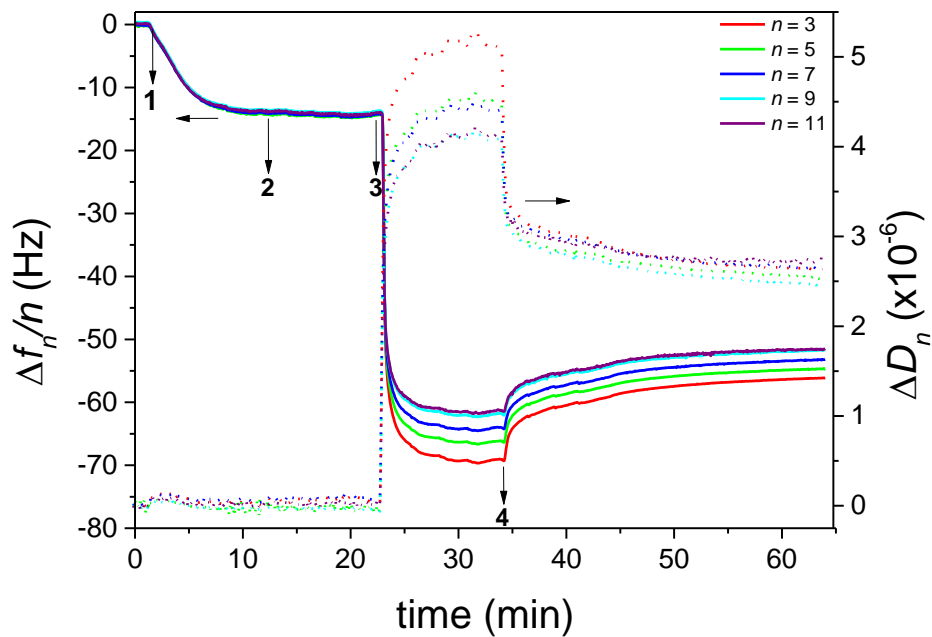
Figure S13: **Representative QCM-D data for the normalised frequency ($\Delta f_n/n$) and dissipation (ΔD_n) shifts** for the adsorption of serum proteins (10% FBS) onto the HS-Pep-1 functionalized Au substrate. Numbers refer to (1) adsorption of HS-Pep-1, (2) rinsing step, (3) adsorption of FBS, (4) rinsing step. A decrease in frequency shift was seen upon addition of FBS, which was partially removed on washing.
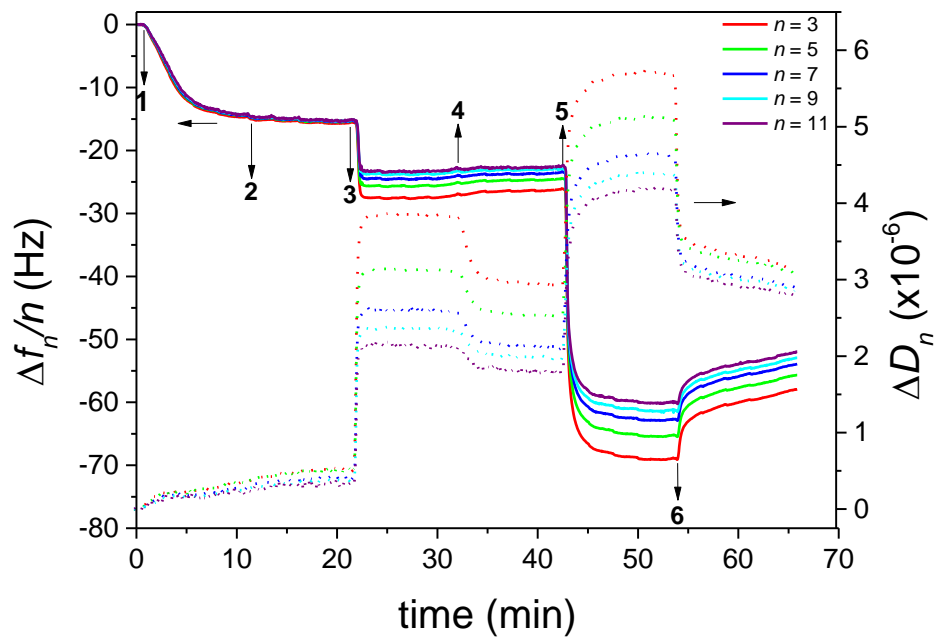
Figure S14: **Representative QCM-D data for the normalised frequency ($\Delta f_n/n$) and dissipation (ΔD_n) shifts** for the adsorption of serum proteins (10% FBS) over the HA layer immobilized on the Pep-1 SAMs. Numbers refer to (1) adsorption of Pep-1, (2) rinsing step, (3) deposition of HA, (4) rinsing step, (5) adsorption of FBS, (6) rinsing step. A decrease in frequency shift was seen upon the addition of FBS, which was partially removed on washing.

Table S1: **Average changes in $\Delta f_7/7$ (Hz) and $\Delta D7$ at the equilibrium, as measured by QCM-D, and modelled thickness (h, nm) and areal mass density (Δm, ng/cm^2),** derived using the the Voigt-based viscoelastic model. All values are the average of 3 independent experiments ± SD.

|	$\Delta f_7/7$ (Hz)	ΔD_7 (x10^{-6})	Voigt Thickness, h_{Voigt} (nm)	Voigt Mass Density, Δm_{Voigt} (ng/cm^2)
Adsorption onto Au				
PLL	-12.4±1.5	0.7±0.3	12.9±3.6	1276.0±366.4
FBS 10%	-18.0±2.4	1.1±0.1	17.2±0.4	1723.3±41.1
Adsorption onto HS-Pep-1				
Alginate (0.5 mg/mL)	-19.7±0.4	4.4±0.3	28.1±2.0	2807.5±192.5
FBS (10%)	-37.5±2.3	2.3±0.2	15.8±0.5	1580.3±49.8
BSA (0.05%)	-18.0±1.0	0.5±0.1	7.4±1.8	710.0±171.9
Adsorption onto HS-Pep-1-HA				
FBS (10%)	-30.6±0.1	0.9±0.1	12.1±6.6	1342.1±653.7
BSA (0.05%)	-12.1±1.7	0.5±0.1	1.8±0.5	185±46
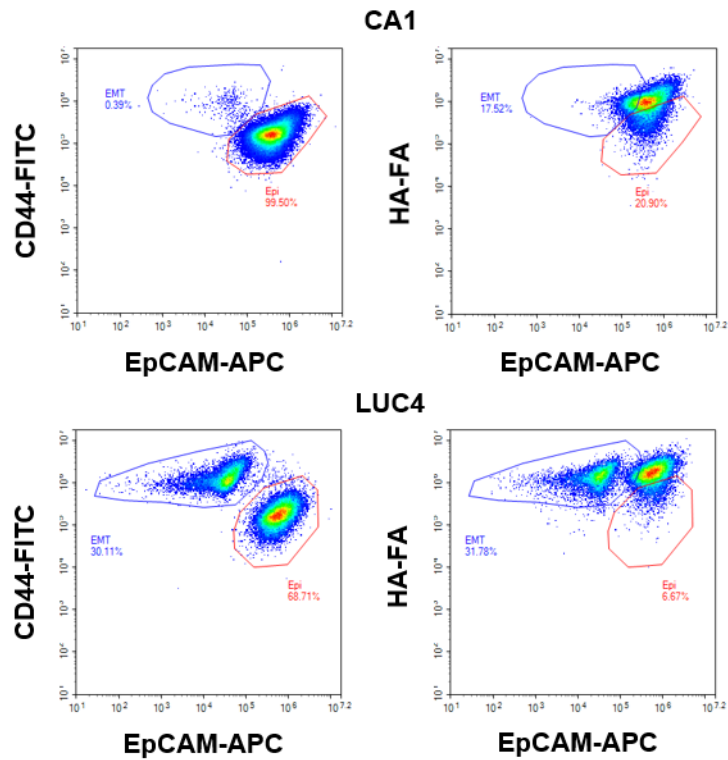
Figure S15: **HA-FA binds to both epithelial and epithelial to mesenchymal transition (EMT) cells for both CA1 and LUC4 cell lines, but the EMT fraction of LUC4 cells is still distinguishable by loss of epithelial cell adhesion molecule (EpCAM) expression.** Flow cytometry scatter plots identifying the epithelial and EMT fractions of CA1 and LUC4 cell lines as CD44^{high} cells that lose EpCAM expression and showing HA-FA binding to CA1 and LUC4 cells.
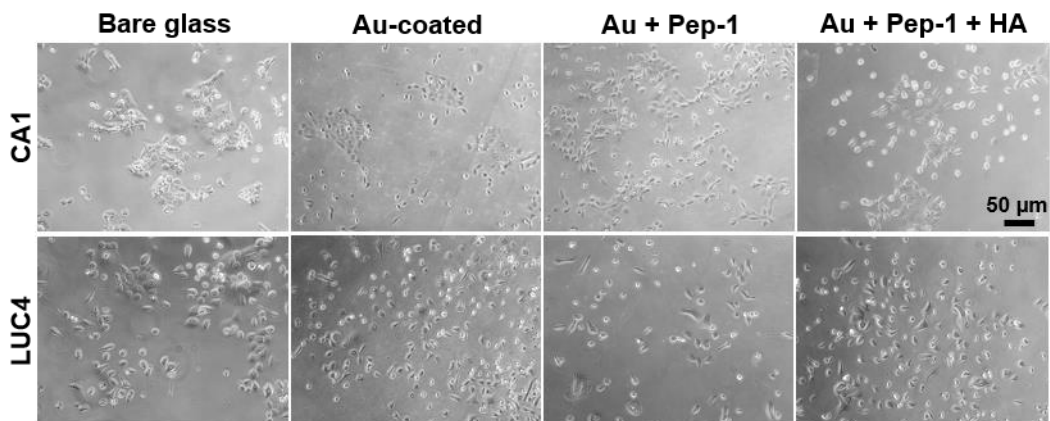

Figure S16: **CA1 and LUC4 cells form colonies on bare glass, with EMT cells present, and are less densely packed, with fewer colonies and greater number of single cells, on the functionalized surfaces.** Bright field microscopy images of CA1 and LUC4 cells cultured on the various surfaces for 4 days. Scale bar is the same for all images.